# Computer Assisted Methods in Engineering and Science

eISSN: 2956-5839 ISSN: 2299-3649

INDEX 324906

Journal published under the auspices of ECCOMAS

Vol. 33
No. 1
2026

Institute of Fundamental Technological Research
Polish Academy of Sciences

# COMPUTER ASSISTED METHODS in ENGINEERING and SCIENCE


eISSN 2956-5839 ISSN 2299-3649
(Instytut Podstawowych Problemów Techniki Polskiej Akademii Nauk
– Institute of Fundamental Technological Research, Polish Academy of Sciences)

## Aims and Scope

*Computer Assisted Methods in Engineering and Science* (CAMES) is a refereed international journal, published quarterly, providing a scientific exchange forum and an authoritative source of information in the field of broadly understood computational engineering and applied sciences. The objective of the journal is to support researchers and practitioners by offering them the means facilitating access to the newest research results reported by leading experts in the field, publication of own contributions and dissemination of information relevant to the scope of the journal which includes three main categories:

- Contributions presenting new research methods of mathematical modeling and computer simulations in engineering and applied sciences, including traditional areas such as solid and structural mechanics, material science, fluid dynamics, acoustics and electromagnetics but going beyond them to account for application relevant issues in physics, chemistry, biology and mathematics, scientific computing, large scale optimization, intelligent systems as well as in multi-scale and multi-physics problems.
- Articles describing novel applications of computational techniques supporting engineering practice and education in areas like mechanical, aerospace, civil, naval, software, chemical and architectural engineering, materials science as well as demonstrations of their practical use in solving real life problems.
- State-of-the-art tutorials, providing the readership with a guidance on important research directions as observed in the current world literature on computer assisted methods in engineering and science.

The journal also publishes book reviews and information on activities of the European Community on Computational Methods in Applied Sciences (ECCOMAS).

## Editorial Board



## Editorial Office

Institute of Fundamental Technological Research, PAS
Pawińskiego 5B, 02-106 Warsaw, Poland
E-mail: cames@ippt.pan.pl, URL: https://cames.ippt.pan.pl

Typesetting in LaTeX: Katarzyna Jezierska Graphic design cover: Mirosław Dziewoński

Institute of Fundamental Technological Research
Polish Academy of Sciences

# COMPUTER ASSISTED METHODS in ENGINEERING and SCIENCE

Volume 33
Issue 1

Guest Editors
Agnieszka Ozimek, Paweł Ozimek

*Computer Assisted Methods in Architecture and Urban Planning*

Warsaw 2026

## Advisory Editorial Board of CAMES

Advisory Editorial Board consists of members of Managing Board of ECCOMAS with co-opted members and chairmen of Technical Committees of ECCOMAS.

*Computer Assisted Methods in Engineering and Science*
**33**(1): 3–5, 2026, https://doi.org/10.24423/cames.2026.33.1.preface

# Preface to the Special Issue on Computer Assisted Methods in Architecture and Urban Planning

We are pleased to present a special issue of *Computer Assisted Methods in Engineering and Science* (CAMES), covering papers focusing on selected aspects of computer-aided design methods in architecture, urban planning, and landscape architecture. The presented content is interdisciplinary in nature, merging many fields and research areas because of the usage of digital tools.

The editors of this issue intended to highlight the beneficial role of computing methods in data acquisition and spatial analysis, while simultaneously considering the saturation of this space with cultural values. The papers included demonstrate the usefulness of these tools from both engineering and humanistic perspectives. We hope that addressing these matters in the CAMES journal will bridge the technological community with the historical and social aspects of space, thereby justifying the necessity for the development of digital tools to support the preservation of this context.

The issue begins with an article titled 'Combining Indoor and Outdoor Positioning for Navigation in AR Environments' by Krzysztof Skabek, Dominika Rola, and Wojciech Zamarski [1], which aims to evaluate augmented reality (AR) technologies – Vuforia, Immersal, MultiSet, and the ARCore Geospatial API. The study examined both the efficacy and accuracy of the results and the resilience to disturbances in location and navigation. The initial phase of the research was conducted in the laboratory, enabling a thorough evaluation of the modules. The subsequent phase took place in a hybrid setting on the Cracow University of Technology (CUT) campus, demonstrating the influence of changing environmental factors on augmented reality navigation performance. The research findings facilitated the development of recommendations for selecting AR localisation platforms for mixed navigation, and a practical implementation was created within the Unity environment.

The next research, entitled 'Digital Tool Supporting the Documentation and Analysis of Cultural Heritage: The Case of the Analytical 3D Model of the Zamość Fortress', written by Michał Wac and Bartosz Szostak [2], describes the approaches used to elaborate digital documentation and, moreover, possibil-

ities to analyse cultural heritage resources on a city scale. The medieval centre of Zamość, Poland, along with its fortifications, has been designated as a UNESCO World Heritage Site and was chosen as an example. Data acquired through terrestrial laser scanning (TLS), unmanned aerial vehicles (UAVs), and terrestrial photogrammetry produced a 3D dataset comprising over 100 buildings and significant elements of public space. The model obtained was organised based on addresses and plot identifiers. Structured parameters were allocated to specific edifices and integrated into the building information model (BIM)/openBIM system. This organised information is useful in conservation diagnostics and the evaluation of urban structural components. The developed method enables functional classification of objects, the assessment of their technical state, and the analysis of energy aspects.

The article, 'The Impact of Point Cloud Simplification on the Accuracy of the Viewshed', authored by Jerzy Orlof and Adrian Widłak [3], focuses on point cloud data, which are very large datasets that require enormous computational power to process. This makes them difficult to implement in practice. The work addresses visibility analysis, specifically viewsheds. Its objective is to assess the accuracy of determining the field of view depending on the degree of the point cloud simplification. Comparing the viewsheds generated using ray tracing on the original dataset and at subsequent levels of simplification enabled an assessment of the acceptable level of data reduction without a significant impact on results of the analyses. Computational time analyses were also conducted to identify the optimal point cloud simplification level in terms of both performance and the obtained results.

In their recent study, 'Possibilities for Obtaining Terrain Models, Orthophoto Maps, and Point Clouds with the Use of a Multirotor UAV', Piotr Łabędź and Paweł Ozimek [4] introduced a method for acquiring spatial data via unmanned aerial vehicles (UAVs). Their investigation involved a hexacopter equipped with a high-end camera capable of recording 4K video and collecting high-resolution images. The subsequent phases of the project involve flights over the analysed object to capture video or a series of photographs. Image processing follows image selection, organisation based on capture location, and subsequent integration to generate a dense point cloud. The resulting structure is subsequently utilised to create a mesh with a variable number of vertices. The photographs serve as the foundation for acquiring textures for polygons. This method provides high-quality terrain and architectural data, with the point cloud being useful for analysis, inventory, accurate model creation, or supplementing less detailed resources.

By presenting you with this special thematic issue, we cordially encourage you to submit your papers, which will enable us to continue this initiative in the form of a series of journal issues devoted to the above-mentioned topics. Sub-

missions may cover any aspects of computer-aided design methods in building architecture, interior, construction, and urban design, landscape architecture, urban planning, and land use, including but not limited to:

- building information model,
- computer-aided design,
- geographic information systems.

Guest Editors

dr hab. inż. arch. Agnieszka Ozimek, prof. PK
*Faculty of Architecture,*
*Cracow University of Technology*
*Cracow, Poland*

dr hab. inż. arch. Paweł Ozimek, prof. PK
*Faculty of Computer Science and Mathematics,*
*Cracow University of Technology*
*Cracow, Poland*

## References

1. Skabek K., Rola D., Zamarski W., Combining indoor and outdoor positioning for navigation in AR environments, *Computer Assisted Methods in Engineering and Science*, **33**(1): 7–25, 2026, https://doi.org/10.24423/cames.2025.1966.
2. Wac M., Szostak B., Digital tool supporting the documentation and analysis of cultural heritage: The case of the analytical 3D model of the Zamość fortress, *Computer Assisted Methods in Engineering and Science*, **33**(1): 27–49, 2026, https://doi.org/10.24423/cames.2025.1943.
3. Orlof J., Widłak A., The impact of point cloud simplification on the accuracy of the viewshed, *Computer Assisted Methods in Engineering and Science*, **33**(1): 51–68, 2026, https://doi.org/10.24423/cames.2025.1936.
4. Łabędź P., Ozimek P., Possibilities for obtaining terrain models, orthophoto maps, and point clouds with the use of a multirotor UAV, *Computer Assisted Methods in Engineering and Science*, **33**(1): 69–81, 2026, https://doi.org/10.24423/cames.2025.273.

*Computer Assisted Methods in Engineering and Science*
**33**(1): 7–25, 2026, https://doi.org/10.24423/cames.2025.1966

# Combining Indoor and Outdoor Positioning for Navigation in AR Environments

Krzysztof Skabek*, Dominika Rola, Wojciech Zamarski

*Faculty of Computer Science and Mathematics, Cracow University of Technology, Kraków, Poland*

* *Corresponding Author: krzysztof.skabek@pk.edu.pl*

This article presents a comparative analysis of augmented reality (AR) technologies – Vuforia, Immersal, MultiSet, and the ARCore Geospatial Application Programming Interface (API) – in terms of performance, accuracy, and interference tolerance for indoor and outdoor positioning and navigation. Two test environments were used: an indoor (laboratory) setup enabling detailed module testing, and a hybrid deployment on the Cracow University of Technology (CUT) campus to illustrate the feasibility of AR navigation in diverse environmental conditions. The research was conducted according to six scenarios. One involved outdoor GPS navigation, while the others concerned indoor navigation. Based on the measurements, recommendations are provided for selecting AR localization platforms for mixed navigation. As part of the detailed testing, an AR navigation system was implemented on the CUT campus as a combination of indoor and outdoor approaches. The final implementation was developed in the Unity environment. Software tests were conducted with particular emphasis on transitions between indoor and outdoor navigation.

**Keywords:** augmented reality (AR), 3D reconstruction, photogrammetry, LiDAR (light detection and ranging), indoor and outdoor positioning, geolocalization.



## 1. Introduction

Accurate positioning is a fundamental requirement for compelling augmented reality (AR) experiences, as it enables virtual objects to be meaningfully integrated with the physical environment. Depending on the context – indoors or outdoors – AR systems employ a variety of localization techniques. Indoor positioning relies on technologies such as visual SLAM (simultaneous localization and mapping) [16, 18], fiducial markers, Wi-Fi [22–24, 44], Bluetooth beacons [26, 27], and UWB (ultra-wideband) [28], while outdoor positioning is pri-

marily based on satellite navigation systems such as GPS (global positioning system), often enhanced with sensor fusion or geospatial visual data. Recent advancements have focused on hybrid solutions that leverage the strengths of multiple technologies, aiming to achieve higher accuracy, robustness, and a seamless user experience across diverse environments [12, 38–40].

Accurate positioning technologies are key enablers for a wide range of AR applications. From indoor navigation in complex environments like airports and museums [1], to outdoor experiences in tourism, urban planning [2], and gaming [3], the ability to precisely locate and anchor virtual objects unlocks new forms of interaction. Positioning in AR also supports innovative solutions in fields such as industrial maintenance [4], medical guidance and training [5, 6], as well as education, marketing, and emergency response, where real-time spatial information enhances both user engagement and operational efficiency. As AR positioning methods continue to advance, they open the door to increasingly immersive and practical experiences across diverse sectors.

Contemporary AR-based navigation solutions transfer the experience of human interaction with the real environment into the virtual world. Inspiring examples include Live View [36] in Google Maps, Sygic GPS Navigation [45], and many others [46–48]. Despite achievements in AR navigation, the Cracow University of Technology campus lacks a dedicated navigation system based on this technology. Therefore, this article focuses on developing an AR mobile application that supports users in finding their way to selected destinations on the campus and within its buildings.

The pre-development stage of the AR navigation system involved a comparative analysis and selection of AR development platforms, with particular emphasis on Vuforia, Immersal, MultiSet, and Geospatial API. Considerable attention was devoted to assessing the suitability of these systems for developing navigation applications by examining their performance, accuracy, and interference tolerance. Experimental studies were conducted in both controlled indoor and outdoor environments to provide a comprehensive understanding of the capabilities and limitations of the tested solutions.

The novelty of this work lies in an end-to-end, scenario-based comparison of four practical AR localization solutions (Vuforia, Immersal, MultiSet, and ARCore Geospatial API) under a single, unified evaluation app and consistent criteria spanning performance, accuracy, and robustness to interference. In addition, we demonstrate a hybrid campus-scale AR navigation prototype that performs automatic indoor–outdoor switching (Area Target vs. Geospatial anchoring) while maintaining a consistent navigation layer (navigation mesh (NavMesh) and points of interest (POIs)) and user experience. The resulting recommendations are grounded in repeatable measurements across six scenarios in both controlled and real-world environments.

## 2. Software for AR localization

Several commercial and research-driven software platforms facilitate AR positioning in both indoor and outdoor scenarios. Vuforia is a widely adopted AR software development kit (SDK) that utilizes marker-based and markerless tracking for robust object registration in varying environments [7, 9, 10]. Immersal provides solutions for large-scale indoor AR experiences, integrating visual positioning and sensor fusion for precise localization in enterprise settings [8]. MultiSet offers advanced multi-sensor data integration for spatial tracking, supporting diverse use cases from interactive exhibitions to industrial applications [13]. These tools represent the state-of-the-art in enabling reliable AR positioning and serve as foundations for many current and emerging AR applications. Other commercial VPS (visual positioning system) options include Lightship VPS by Niantic [34].

### *2.1. Vuforia*

Vuforia Engine developed by Parametric Technology Corporation (PTC) is a mature AR platform for Android, iOS, the Universal Windows Platform (UWP), Unity, and headsets (HoloLens 2, Magic Leap 2). It offers robust tracking and recovery after brief target loss, supporting seamless AR experiences. A key feature in this study is Area Targets, which use full 3D scans (e.g., via Vuforia Creator and LiDAR (light detection and ranging) devices) to localize the camera within indoor spaces [10]. This turns interiors into spatial references for placing AR content. Area Targets are intended for indoor use; outdoor performance is limited by lighting and occlusions. Other tracking modes include: Image Targets – 2D images as anchors, Model Targets – 3D object detection by geometry, VuMarks – custom markers encoding data and *Ground Plane* – horizontal surface detection. Vuforia supports multiple simultaneous targets and many devices. Main limitations include: no native GPS/geolocation for outdoor navigation, performance depends on sensor quality and target preparation, and the free license limits the number of trackables.

### *2.2. Immersal*

The Immersal SDK provides markerless spatial mapping and 6 degrees of freedom (DoF) localization via point cloud maps [37], with reported centimeter-level precision [16, 17]. Mapping works on ARKit/ARCore smartphones or with 360° cameras or LiDAR capture; spatial data can be exported as meshes or embedded for offline use. Localization runs via the cloud (online) or using on-device maps (offline). Immersal has been used in both indoor and outdoor environments (e.g., malls, industry, campuses). Multiple datasets can be merged to

support building- or campus-scale navigation. Accuracy depends on careful image acquisition and environmental stability (lighting, motion), but deployment is simplified by using standard mobile cameras. Unity integration and sample scenes speed up prototyping. A free non-commercial tier (e.g., map/image limits, branding) is available, while larger projects require paid plans.

### *2.3. MultiSet*

MultiSet AI is a VPS using deep learning and high-resolution 3D mapping for 6DoF localization with centimeter-level precision. It targets scales from rooms to large facilities and processes LiDAR scans into vector representations, enabling robust localization. Computation is primarily cloud-based, requiring internet connectivity. A dedicated iOS app (LiDAR) generates 3D meshes for object placement and occlusion; multiple datasets can be fused for complex sites. The system is suitable for indoor navigation and industrial scenarios, including visualization of building information modeling (BIM) and Internet of Things (IoT) data. A basic free plan (with limits) supports commercial use, while extended plans cater to enterprise deployments.

### *2.4. Geospatial API*

Google's ARCore Geospatial API [11, 36] enables global-scale AR by combining GPS, device sensors, and Google's visual positioning. Developers place anchors using WGS84 (latitude, longitude, altitude) on outdoor surfaces. SDKs support Android/iOS and Unity (via AR Foundation, ARCore Extensions) with localization performed via the cloud. The API refines GPS using visual matches to Street View imagery [17, 20, 40], achieving accuracy within tens of centimeters under favorable conditions [15, 21]. ARCore adds SLAM tracking, plane detection, lighting estimation, depth-based occlusion [41], and Cloud Anchors for multiuser experiences. Limitations include: unsuitability for indoor environments (GPS degradation, lack of Street View coverage) and performance depends on imagery quality, lighting, and weather. Access is free within quotas, making it effective for wide-area outdoor AR applications (navigation, tourism, urban information).

### *2.5. Selecting the solutions*

The examined AR platforms differ in their underlying positioning technologies, environmental adaptability, and deployment workflows, which influences their applicability in both indoor and outdoor AR scenarios.

Vuforia is a well-established AR engine offering multiple tracking modes, including Area Targets and Model Targets, based on preprocessed images and

3D scans. It provides robust indoor localization on a broad range of devices but lacks support for GPS-based positioning and is not officially intended for outdoor use. Its performance depends heavily on the quality of input assets and camera sensors, and the free license imposes restrictions on the number of supported targets.

Immersal utilizes a markerless VPS that builds point cloud maps from captured images, supporting centimeter-level accuracy in both indoor and outdoor environments. It allows for online or offline localization, and map creation can be performed using mobile devices or dedicated scanners. Its flexibility, combined with wide hardware compatibility, makes it suitable for large-scale spatial mapping without specialized equipment.

MultiSet also operates on visual positioning principles but enhances spatial understanding through deep learning and vectorized 3D representations. It offers high accuracy and contextual scene analysis, although it currently supports only iOS devices with LiDAR for map generation. Localization requires active internet connectivity, and cloud-based processing is central to its operation.

Geospatial API combines GPS, sensor data, and Google's visual localization to provide outdoor positioning without prior mapping. It supports large-scale deployment and enables fast prototyping, though performance is dependent on environmental conditions and the availability of Street View imagery. The system does not support indoor use and requires a constant internet connection.

All platforms offer integration with Unity and provide tools for 3D content alignment, yet they differ in licensing terms, mapping requirements, and environmental robustness. Immersal and MultiSet offer detailed localization in controlled or complex spaces, while Geospatial API excels in rapid deployment across urban outdoor environments. Vuforia remains a reliable solution for structured indoor contexts where predefined assets are available. It is worth noting that some previously popular services have been discontinued (e.g., Azure Spatial Anchors was retired in 2024) [35].

## 3. Preparing the environment

### *3.1. Unity and libraries*

To develop an AR application enabling the testing of positioning technologies in both indoor and outdoor environments, the Unity engine was used – one of the most widely adopted platforms for creating immersive applications.

The AR functionality was implemented using the AR Foundation package [19], which provides a unified interface for the native ARCore (Android) and

ARKit (iOS) libraries. The project also integrated the following libraries and extensions:

- ARCore extensions – enabling the use of features such as Geospatial API and Cloud Anchors,
- ARKit plugin – providing full support for devices running iOS,
- ARCore – supporting Android devices and offering core tracking and localization functionality in AR environments,
- Vuforia Engine – the project utilized the Area Target feature, allowing for scanning and subsequent recognition of physical spaces based on previously generated 3D models. This solution enabled precise user positioning within known environments, even in the absence of a GPS signal,
- Immersal SDK – leveraging visual SLAM mechanisms for localization and spatial mapping in both indoor and outdoor environments,
- MultiSet plugin – a cloud-based AR positioning system that utilizes LiDAR scans and deep learning to enable precise 6DoF localization in complex indoor environments.

The source code was developed using the Visual Studio 2022 development environment. Builds were prepared for both Android and iOS platforms, and the application was tested on mobile devices.

The application configuration also included appropriate system permissions, such as access to GPS and inertial sensors. When enabling advanced Wi-Fi RTT (Wi-Fi round-trip time) features, privacy-preserving approaches should be considered [25].

This development environment enabled efficient integration and comparison of various positioning solutions in the context of AR applications, while maintaining high cross-platform compatibility and operational performance.

## 4. Positioning accuracy

All experiments were conducted using a unified testing app built in Unity. The primary indoor testing site was a controlled $3\,\mathrm{m} \times 3\,\mathrm{m}$ room with standardized lighting and reference markers, illustrated as in Fig. 1. Outdoor measurements were conducted on a paved square at the university campus.

To prepare the AR models, 3D scans (or photos for the Immersal platform) were created using dedicated applications (Vuforia Creator, Immersal Mapper, MultiSet) on an iPhone 15 Pro 128GB, which is equipped with a LiDAR sensor. The Unity environment views of the prepared scenes for each platform are shown in Fig. 2. At this stage of development, the position of each cube is correct, meaning that the base of each object aligns with the drawn reference square.

FIG. 1. Testing room.

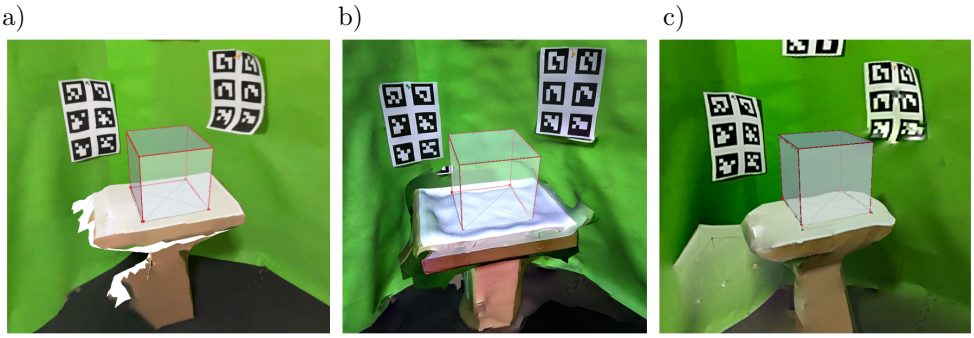


FIG. 2. Views from Unity showing the placement of the virtual cube in the mapped space for the AR platforms: a) Vuforia, b) Immersal, c) MultiSet.

### *4.1. Initial model accuracy*

At first, we compared the accuracy of three mesh models prepared for embedding virtual objects in augmented environments: Vuforia, Immersal and MultiSet. Vuforia and MultiSet use LiDAR range measurements to obtain the initial model of the surrounding area. Immersal, on the other hand, establishes the model based on photogrammetry [37]. The numbers of vertices obtained for our indoor scene are indicated in Fig. 3. It appears that the densest model was created using photogrammetry. In the case of LiDAR measurements, the initial point clouds are more regular and dense, but the final mesh representation stored in the AR application is optimized [31–33].

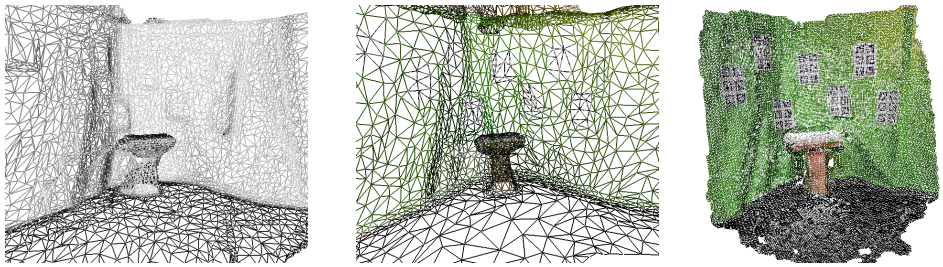

Vuforia
6346 vertices

MultiSet
3455 vertices

Immersal
24 740 vertices

Fig. 3. Initial meshes with their numbers of vertices.

### *4.2. Comparison criteria*

To assess the positioning capabilities of the AR technologies tested (Vuforia, Immersal, MultiSet, and Geospatial API), a comprehensive set of evaluation criteria was established and grouped into three categories: performance, accuracy, and resistance. Most criteria were quantitative, except for two qualitative ones: the effect of colored lighting (3.2) and tolerance to projected patterns (3.3).

1. Performance:
   - 1.1. Scene recognition time: time (in seconds) from app launch to the initial appearance of an AR object.
   - 1.2. Battery consumption: average percentage drop in battery level per minute of continuous use.
   - 1.3. Memory usage: random-access memory (RAM) usage measured with the PSS (proportional set size) metric.
2. Accuracy:
   - 2.1. Indoor initial positioning error: mean distance between AR and real-world marker vertices in a 20 cm reference square.
   - 2.2. Outdoor positioning error: same as 2.1, measured against a 150 cm reference square in an outdoor environment.
   - 2.3. Extended tracking error: positioning error of a secondary virtual cube located 5, 10, and 30 meters from the originally mapped scene. This criterion evaluates the system's ability to maintain accurate spatial tracking despite moving through unmapped areas or losing visual contact with the reference scene.
   - 2.4. Positional drift over time: maximum deviation recorded during a 10-minute session of continuous AR tracking in a static position.
3. Resistance:
   - 3.1. Low-light threshold: maximum percentage reduction in brightness at which the AR system still functions.

3.2. Colored lighting impact: binary value indicating whether AR initialization succeeds under colored red–green–blue (RGB) lighting conditions.

3.3. Pattern robustness: binary value indicating whether the AR system can recognize scenes under projected high-contrast black-and-white patterns.

### *4.3. Measurement methodology*

Six testing scenarios were defined:

Scenario I: measured scene recognition time, indoor positioning error, and positional drift. The smartphone was placed at three distinct positions (A, B, and C), each representing a different level of marker visibility and spatial challenge:

- position A: all reference markers were fully visible, creating optimal tracking conditions,
- position B: approximately half of the markers were occluded, representing moderate difficulty for AR tracking,
- position C: only a few markers were visible, presenting a minimal-information scenario and testing the boundary of reliable tracking.

Scenario II: evaluated battery and memory consumption over a 30-minute session of uninterrupted app operation. Data were logged using diagnostic scripts.

Scenario III: assessed extended tracking accuracy by placing a secondary AR cube at 5, 10, and 30 meters from the original scene. Users moved through these locations while maintaining line-of-sight camera input. The error was calculated relative to a reference square at each distance. In scenario III, extended tracking across 5 m, 10 m, and 30 m relies on persistent visual localization and place recognition [17] to mitigate drift outside the originally mapped area.

Scenario IV: determined the minimum ambient light required for successful recognition by incrementally increasing brightness from total darkness.

Scenario V: evaluated resistance under RGB lighting and projected black-and-white patterns. Recognition success under altered visuals was recorded.

Scenario VI: measured outdoor accuracy using a 150 cm square on the pavement. Positioning error was calculated after stabilization of AR tracking during walking.

Tests were conducted on a Samsung Galaxy S24 (Exynos 2400, 8 GB RAM, Android 14). Each measurement was repeated ten times. The device was mounted on a tripod for all tests except those requiring user movement.

### *4.4. Performance*

Performance was evaluated in terms of scene recognition time (scenario I), battery consumption, and RAM usage (scenario II). In the recognition speed test, both Vuforia and Immersal demonstrated rapid initialization across all positions (A–C), with mean detection times ranging from 1.65 to 2.51 seconds. Vuforia was particularly consistent across conditions, showing minimal variance even under reduced marker visibility. In contrast, MultiSet exhibited a considerably higher and less stable recognition times, peaking at 9.90 ±1.30 seconds in position A, and only slightly improving in position C (see Table 1).

Table 1. Scene recognition time in seconds in scenario I.

| Position | Vuforia | | Immersal | | MultiSet | |
|---|---|---|---|---|---|---|
| | Mean | Standard deviation | Mean | Standard deviation | Mean | Standard deviation |
| A | 1.69 | 0.36 | 1.65 | 0.31 | 9.90 | 1.30 |
| B | 1.66 | 0.30 | 1.65 | 0.29 | 9.66 | 2.28 |
| C | 1.87 | 0.75 | 2.51 | 0.29 | 7.72 | 0.39 |

Battery and memory efficiency were assessed over a 30-minute continuous operation (scenario II). Vuforia showed the highest battery consumption at 0.45 %/min, while Immersal consumed slightly less (0.433 %/min) but used the most RAM with 717 MB PSS. MultiSet was the most resource-efficient, consuming just 0.367 %/min of battery and 458 MB of memory, making it a better choice for power-constrained or long-duration mobile AR tasks.

### *4.5. Accuracy*

Accuracy testing spanned several scenarios and criteria, including indoor and outdoor initial positioning, tracking drift, and extended tracking at various distances. In scenario I (initial indoor positioning), Vuforia and Immersal delivered stable results with positioning errors generally below 4 cm. MultiSet matched this performance in optimal conditions (positions A and B) but deteriorated severely in position C, where error rose dramatically to over 61 cm, indicating poor robustness to reduced feature visibility (see Table 2).

Table 2. Initial AR positioning error in indoor scenario [cm].

| Position | Vuforia | | Immersal | | MultiSet | |
|---|---|---|---|---|---|---|
| | Mean | Standard deviation | Mean | Standard deviation | Mean | Standard deviation |
| A | 3.55 | 0.57 | 3.35 | 1.88 | 2.84 | 1.45 |
| B | 2.57 | 0.29 | 1.21 | 0.43 | 2.84 | 1.66 |
| C | 3.61 | 0.24 | 1.43 | 0.92 | 61.69 | 3.46 |

In extended tracking (scenario III), where AR targets were located at 5 m, 10 m, and 30 m away from the origin, Vuforia yielded the lowest errors at short distances, while Immersal performed better at 30 m, suggesting better spatial persistence at scale. MultiSet showed relatively high and fluctuating errors across all distances. These observations align with recent advances in VIO (visual-inertial odometry) robustness and event-based fusion for odometry [29, 30]. These results are also in line with patterns observed on public benchmarks for VO (visual odometry)/SLAM [42, 43].

In outdoor testing (scenario VI), Immersal again led with 9.4 cm average error. Vuforia and MultiSet followed with 16.2 cm and 19.1 cm, respectively. Geospatial API performed poorly due to GPS limitations, with average error exceeding 3.2 meters [15, 21].

Drift testing over a 10-minute period confirmed the stability of Vuforia and Immersal (maximum drift below 12 cm), while MultiSet's error in position C reached nearly 89 cm, reinforcing earlier findings of instability in complex environments.

### *4.6. Resistance*

The resistance of AR systems to environmental challenges was tested in low-light conditions (scenario IV) and under visual interference (scenario V). In reduced lighting, Immersal retained functional tracking down a 92 % luminance reduction, outperforming Vuforia (90 %) and MultiSet (82 %), indicating better sensor robustness and image processing under poor visibility (see Table 3).

Table 3. Maximum luminance reduction tolerated before failure.

| Platform | Vuforia | | Immersal | | MultiSet | |
|---|---|---|---|---|---|---|
| Reduction [%] | Mean | Standard deviation | Mean | Standard deviation | Mean | Standard deviation |
| | 90 | 0.89 | 92 | 1.64 | 82 | 6.46 |

Under RGB lighting, all systems functioned correctly, demonstrating color-independence. However, in the presence of high-contrast projected patterns, only Vuforia was able to consistently initialize and maintain AR tracking. Immersal and MultiSet failed under three of the four tested patterns, exposing a lower tolerance to structured visual noise.

## 5. Implementation of AR navigation system

The presented application was developed as part of a master's thesis [14] with the goal of testing and evaluating the effectiveness of AR-based positioning

systems in real-world educational settings. The prototype serves as a proof of concept for a system that assists users in locating specific destinations across the Cracow University of Technology (CUT) campus, combining indoor and outdoor localization methods in a single interface.

The system was implemented using the Unity game engine and integrates two complementary AR technologies. For indoor spaces, the Vuforia Engine was used, leveraging 3D scans of building interiors to provide accurate camera tracking and virtual content placement. For outdoor areas, the application employs the Google Geospatial API, which uses a combination of GPS and visual localization through Street View data to estimate device position on a global scale.

Figure 4 summarizes the runtime workflow in three cooperating layers. First, based on the current user position in the localization system, the appropriate tracking method is selected: indoor via Vuforia Area Target or outdoor via Geospatial API. Once localization is successful, the user position is passed to the navigation system to compute the route on a navigation mesh (NavMesh). Then, the user moves to another localization following turn-by-turn guidance

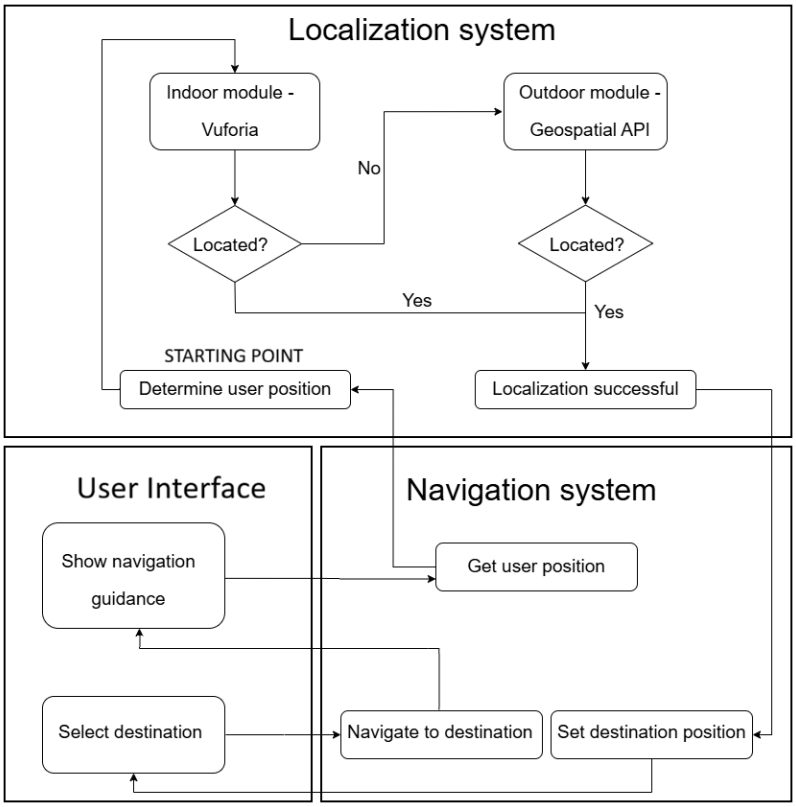


Fig. 4. System architecture and data flow.

provided through the user interface (UI). This separation simplifies automatic indoor/outdoor mode switching and keeps a consistent user experience regardless of the underlying localization method.

Outdoor positioning, illustrated in Fig. 5, exhibited lower precision. Virtual objects were occasionally offset from their intended locations, which affected the clarity of spatial feedback. This behavior was most noticeable in areas with limited satellite visibility or outdated visual data. Nevertheless, the system remained functional and responsive, providing general orientation cues.

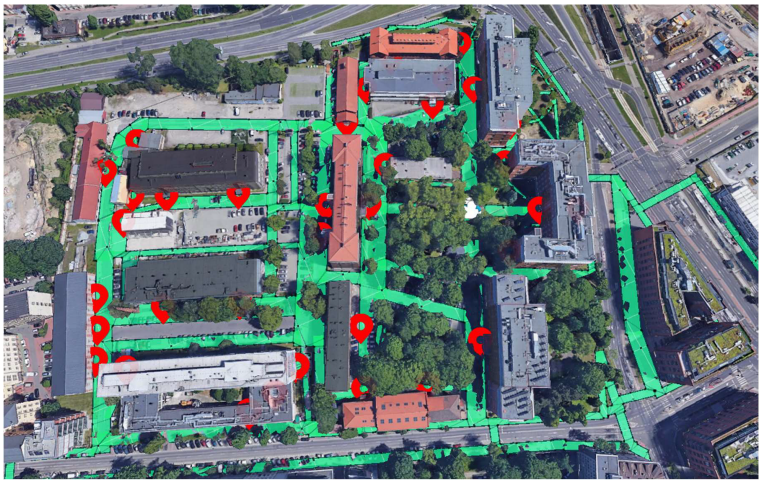

FIG. 5. Outdoor navigation map: NavMesh (green) and POIs (red markers) on the campus grounds.

To make navigation possible, a NavMesh (Unity AI navigation) was prepared to cover continuous, walkable surfaces–outdoors (walkways, plazas) and indoors (corridors, stairwells). On top of this navigation layer, POIs are placed as Unity objects used as destinations and reference points. Outdoors, each POI is georeferenced with WGS84 (World Geodetic System 1984) coordinates (latitude/longitude/altitude) and anchored as an ARCore Geospatial Anchor (with heading). Indoors, POIs are defined in the local frame of the Vuforia Area Target scan (3D coordinates in model space). Mode switching is automatic: when stable Area Target tracking is present, the app enables Indoor mode (geospatial anchors are disabled and cleared); otherwise, if geolocation conditions are met, Outdoor mode is activated. Examples of the outdoor and indoor configurations of the NavMesh and POIs are shown in Figs. 5 and 6, respectively.

In practical use, the application automatically switches between indoor and outdoor localization depending on the user's current context. This hybrid model enables continuous positioning across diverse spatial environments. Indoor localization was generally accurate and stable, especially in the scanned areas of

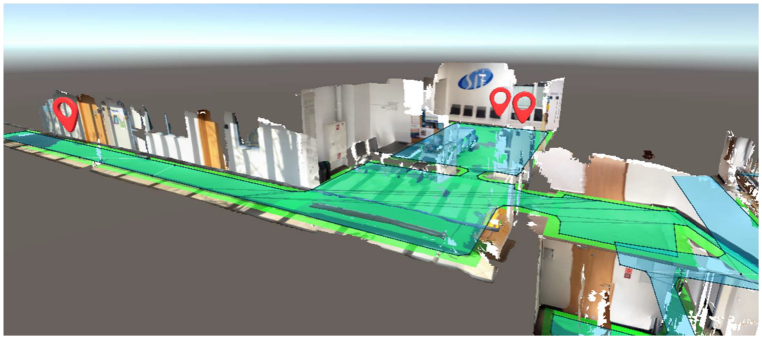

Fig. 6. Indoor navigation map: NavMesh (green) and POIs (red markers) inside the building (Area Target).

the WIiTCH building. As shown in Fig. 7, AR elements such as arrows and lines were correctly positioned and maintained spatial consistency during use.


Fig. 7. Screenshots from our AR system: a) indoor navigation, b) outdoor navigation.

Overall, testing confirmed that the application operates in accordance with the initial design objectives. It provides a working demonstration of AR-based positioning across both indoor and outdoor environments using off-the-shelf technologies. While the system performs well in structured indoor spaces, its

outdoor performance may benefit from the integration of alternative localization methods or the use of more detailed visual mapping. The current version offers a solid foundation for future development and practical deployment in academic or public environments.

## 6. Summary

In this work, we benchmarked multiple widely used AR localization technologies under unified scenarios and demonstrated a hybrid navigation pipeline with seamless indoor–outdoor transitions implemented in Unity. Two test environments were created as part of this work: first, an experimental environment, enabling detailed module testing, and the other, an implementation environment, realized on the Cracow University of Technology campus. Considerable attention was devoted to detailed testing of performance, accuracy, and resistance to interference, including six test scenarios. One of these scenarios involved outdoor GPS navigation, while the others involved indoor visual navigation.

The experiments demonstrated that the tested technologies are generally suitable for use in navigation applications based on AR. Regarding the quality of the initial mesh representation, there is a certain advantage of the LiDAR-based technology providing more regular mesh structures while photogrammetric technology allows for wider use on smartphones equipped only with cameras and in outdoor environments beyond the measurement range of LiDAR sensors.

Analyzing the resistance of the systems to adverse environmental conditions, it was revealed that Vuforia performed particularly well in the presence of visual interference in the form of structured lights. On the other hand, Immersal showed the greatest tolerance to low lighting levels, making this technology particularly attractive for night applications or in poorly lit indoor spaces. In terms of performance, there was a noticeable difference in the time of initializing space tracking, because MultiSet needed significantly more time to recognize the scene than competing solutions, while it had the lowest consumption of system resources. Battery consumption was relatively high for all tested technologies, which could negatively affect the comfort of practical use of AR applications.

The resulting AR application makes it possible to navigate in both indoor or outdoor environments, adapting its navigation routines based on available scope of data, which makes the navigation possible under all conditions considered in this study.

## References

1. Alarifi M.A. *et al.*, Ultra wideband indoor positioning technologies: Analysis and recent advances, *Sensors*, **16**(5): 707, 2016, https://doi.org/10.3390/s16050707.

2. Reitmayr P., Schmalstieg D., Location Based Applications for Mobile Augmented Reality, [In:] *Proceedings of the Fourth Australasian User Interface Conference on User Interfaces 2003*, Vol. 18, pp. 65–73, Australian Computer Society, 2003.

3. Rauschnabel M., Rossmann A., tom Dieck T., An adoption framework for mobile augmented reality games: The case of Pokémon GO, *Computers in Human Behavior*, **76**: 276–286, 2017, https://doi.org/10.1016/j.chb.2017.07.030.

4. Nee A.Y.C., Ong S.K., Chryssolouris G., Mourtzis D., Augmented reality applications in design and manufacturing, *CIRP Annals*, **61**(2): 657–679, 2012, https://doi.org/10.1016/j.cirp.2012.05.010.

5. Vávra M. *et al.*, Recent development of augmented reality in surgery: A review, *Journal of Healthcare Engineering*, **2017**: 4574172, 2017, https://doi.org/10.1155/2017/4574172.

6. Buttiglione M.D., Guerrera F., Piazzolla P., Colombo G., Ruffini E., Gribaudo M., Collaborative virtual reality framework for surgical training and simulation, [In:] *39th Proceedings of ECMS 2025*, Vol. 39, Iss. 1, pp. 661–667, Catania, Italy, 2025, https://doi.org/10.7148/2025-0661.

7. Billinghurst M., Clark A., Lee G., A survey of augmented reality, *Foundations and Trends in Human-Computer Interaction*, **8**(2–3): 73–272, 2015, https://doi.org/10.1561/1100000049.

8. Immersal, Immersal SDK Documentation, 2023, https://developers.immersal.com/docs/ [accessed: 29.05.2025].

9. PTC, Vuforia Engine Library, 2024, https://library.vuforia.com [accessed: 29.05.2025].

10. PTC, *Area Targets*, Vuforia Engine Library, 2021, https://library.vuforia.com/features/area-targets.html [accessed: 10.09.2025].

11. Google, ARCore Geospatial API Documentation, 2024, https://developers.google.com/ar [accessed: 29.05.2025].

12. Guo X., Ansari N., Hu F., Shao Y., Elikplim N.R., Li L., A survey on fusion-based indoor positioning, *IEEE Communications Surveys & Tutorials*, **22**(1): 566–594, 2020, https://doi.org/10.1109/COMST.2019.2951036.

13. MultiSet AI, MultiSet AI Developer Documentation, 2025, https://docs.multiset.ai [accessed: 29.05.2025].

14. Zamarski W., *Navigation methods in augmented reality on the example of the CUT campus*, Master Thesis, Cracow University of Technology, Cracow, 2025.

15. Sattler T. *et al.*, Benchmarking 6DOF outdoor visual localization in changing conditions, [In:] Proceedings of the 2018 IEEE/CVF Conference on Computer Vision and Pattern Recognition, pp. 8601–8610, Salt Lake City, USA, 2018, https://doi.org/10.1109/CVPR.2018.00897.

16. Mur-Artal R., Tardós J.D., ORB-SLAM2: An open-source SLAM system for monocular, stereo, and RGB-D cameras, *IEEE Transactions on Robotics*, **33**(5): 1255–1262, 2017, https://doi.org/10.1109/TRO.2017.2705103.

17. Arandjelović R., Gronat P., Torii A., Pajdla T., Sivic J., NetVLAD: CNN architecture for weakly supervised place recognition, *IEEE Transactions on Pattern Analysis and Machine Intelligence*, **40**(6): 1437–1451, 2018, https://doi.org/10.1109/TPAMI.2017.2711011.

18. Hess W., Kohler D., Rapp H., Andor D., Real-time loop closure in 2D LIDAR SLAM, [In:] *IEEE ICRA Workshop*, 2016, https://research.google.com/pubs/archive/45466.pdf.

19. Unity Technologies, AR Foundation Documentation, 2025, https://docs.unity3d.com/Packages/com.unity.xr.arfoundation@latest/ [accessed: 10.09.2025].

20. Reinhardt T., Using Global Localization to Improve Navigation, *Google Research*, Feb 11, 2019, https://research.google/blog/using-global-localization-to-improve-navigation/ [accessed: 10.09.2025].

21. Hakamäki S., *Assessing Localization Accuracy of Google ARCore Geospatial API*, MSc Thesis, Tampere University, 2024, https://trepo.tuni.fi/bitstream/handle/10024/157627/Hakam%C3%A4kiSaku.pdf.

22. Qiao J., Yang F., Liu J., Huang G., Zhang W., Li M., Advancements in indoor precision positioning: A comprehensive survey of UWB and Wi-Fi RTT positioning, *Network*, **4**(4): 545–566, 2024, https://doi.org/10.3390/network4040027.

23. Kosek-Szott K., Szott S., Ciezobka W., Wojnar M., Rusek K., Segev J., Indoor positioning with Wi-Fi location: A survey of IEEE 802.11mc/az/bk fine timing measurement research, *Computer Communications*, **247**: 108400, 2026, https://doi.org/10.1016/j.comcom.2025.108400.

24. Hashem O., Harras K.A., Youssef M., Accurate indoor positioning using IEEE 802.11mc round trip time, *Pervasive and Mobile Computing*, **75**: 101416, 2021, https://doi.org/10.1016/j.pmcj.2021.101416.

25. Schepers D., Ranganathan A., Privacy-preserving positioning in Wi-Fi fine timing measurement, *Proceedings on Privacy Enhancing Technologies*, **2022**(2): 325–343, 2022, https://crysp.petsymposium.org/popets/2022/popets-2022-0048.pdf.

26. Bai L., Ciravegna F., Bond R., Mulvenna S., A low cost indoor positioning system Using Bluetooth Low Energy, *IEEE Access*, **8**: 136858–136871, 2020, https://doi.org/10.1109/ACCESS.2020.3012342.

27. Bencak P., Hercog D., Lerher T., Indoor positioning system based on Bluetooth Low Energy for intralogistics, *Electronics*, **11**(3): 308, 2022, https://doi.org/10.3390/electronics11030308.

28. Cho J., Jeong S., Kim J.-Y., Kim G.-H., Lee J., Lee B., Real-time indoor localization and safety applications using UWB, *KSCE Journal of Civil Engineering*, **29**(8): 100164, 2025, https://doi.org/10.1016/j.kscej.2025.100164.

29. Minervini A., Carrio A., Guglieri G., Enhancing Visual–Inertial Odometry robustness and accuracy in challenging environments, *Robotics*, **14**(6): 71, 2025, https://doi.org/10.3390/robotics14060071.

30. Zhang J., Yu X., Sier H., Zhang H., Westerlund T., Event-based sensor fusion and application on odometry: A survey, *arXiv*, 2024, https://arxiv.org/abs/2410.15480.

31. Teo T.-A., Yang C.-C., Evaluating the accuracy and quality of an iPad Pro's built-in LiDAR for BIM, *Developments in the Built Environment*, **14**: 100169, 2023, https://doi.org/10.1016/j.dibe.2023.100169.

32. Abdel-Majeed H.M., Shaker I.F., Abdel-Wahab A.M., Awad A.A.D.I., Indoor mapping accuracy comparison between Apple pro devises' LiDAR sensor and terrestrial laser scanner, *HBRC Journal*, **20**(1): 915–931, 2024, https://doi.org/10.1080/16874048.2024.2408839.

33. Sheshtar F.M., Alhatlani W.M., Moulden M., Kim J.H., Comparative analysis of LiDAR and photogrammetry for 3D crime scene reconstruction, *Applied Sciences*, **15**(3): 1085, 2025, https://doi.org/10.3390/app15031085.

34. Niantic, Visual Positioning System (VPS) Documentation, 2025, https://lightship.dev/docs/ardk/features/lightship_vps/ [accessed: 10.09.2025].

35. Microsoft, Azure Spatial Anchors – Product Lifecycle (Retired Nov 20, 2024), 2025, https://learn.microsoft.com/en-us/lifecycle/products/azure-spatial-anchors [accessed: 10.09.2025].

36. Google, Build global-scale, immersive, location-based AR experiences with the ARCore Geospatial API, 2025. https://developers.google.com/ar/develop/geospatial [accessed: 10.09.2025].

37. Schönberger J.L., Frahm J.-M., Structure-from-motion revisited, [In:] *2016 IEEE Conference on Computer Vision and Pattern Recognition*, pp. 4104–4113, 2016, https://openaccess.thecvf.com/content_cvpr_2016/papers/Schonberger_Structure-From-Motion_Revisited_CVPR_2016_paper.pdf.

38. DeTone D., Malisiewicz T., Rabinovich A., SuperPoint: Self-supervised interest point detection and description, [In:] *2018 IEEE Conference on Computer Vision and Pattern Recognition Workshops*, pp. 337–349, 2018, https://openaccess.thecvf.com/content_cvpr_2018_workshops/papers/w9/DeTone_SuperPoint_Self-Supervised_Interest_CVPR_2018_paper.pdf.

39. Sarlin P.-E., DeTone D., Malisiewicz T., Rabinovich A., SuperGlue: Learning feature matching with graph neural networks, [In:] *IEEE Conference on Computer Vision and Pattern Recognition*, pp. 4938–4947, 2020, https://openaccess.thecvf.com/content_CVPR_2020/papers/Sarlin_SuperGlue_Learning_Feature_Matching_With_Graph_Neural_Networks_CVPR_2020_paper.pdf.

40. Sarlin P.-E., Cadena C., Siegwart R., Dymczyk M., From coarse to fine: Robust hierarchical localization at large scale, [In:] *IEEE Conference on Computer Vision and Pattern Recognition*, pp. 12716–12725, 2019, https://openaccess.thecvf.com/content_CVPR_2019/papers/Sarlin_From_Coarse_to_Fine_Robust_Hierarchical_Localization_at_Large_Scale_CVPR_2019_paper.pdf.

41. Du R. *et al.*, DepthLab: Real-time 3D interaction with depth maps for mobile augmented reality, [In:] *UIST '20: Proceedings of the 33rd Annual ACM Symposium on User Interface Software and Technology*, pp. 829–843, 2020, https://doi.org/10.1145/3379337.3415881.

42. Sturm J., Engelhard N., Endres F., Burgard W., Cremers D., A Benchmark for the Evaluation of RGB-D SLAM Systems, [In:] *2012 IEEE/RSJ International Conference on Intelligent Robots and Systems*, pp. 573-580, Vilamoura-Algarve, Portugal, 2012, https://doi.org/10.1109/IROS.2012.6385773.

43. Geiger A., Lenz P., Urtasun R., Are we ready for autonomous driving? The KITTI vision benchmark suite, [In:] *Conference on Computer Vision and Pattern Recognition*, 2012, https://www.cvlibs.net/publications/Geiger2012CVPR.pdf.

44. IEEE, *IEEE Standard for Information Technology–Telecommunications and Information Exchange between Systems Local and Metropolitan Area Networks–Specific Requirements Part 11: Wireless LAN Medium Access Control (MAC) and Physical Layer (PHY) Specifications Amendment 4: Enhancements for Positioning*, 2022, https://standards.ieee.org/ieee/802.11az/7226/.

45. Sygic, Real View Navigation, https://www.sygic.com/what-is/real-view-navigation.

46. Huang B.-C., Hsu J., Chu E.T.-H., Wu H.-M., ARBIN: Augmented Reality Based Indoor Navigation System, *Sensors*, **20**(20): 5890, 2020, https://doi.org/10.3390/s20205890.

47. Sato F., Indoor navigation system based on augmented reality markers, [In:] Barolli L., Enokido T. [Eds.], *Innovative Mobile and Internet Services in Ubiquitous Computing. IMIS 2017*, Advances in Intelligent Systems and Computing, Vol. 612, pp. 266–274, Springer, Cham, 2018, https://doi.org/10.1007/978-3-319-61542-4_25.

48. Jiang J.R., Subakti H., An indoor location-based augmented reality framework, *Sensors*, **23**(3): 1370, 2023, https://doi.org/10.3390/s23031370.

*Received October 30, 2025; revised December 23, 2025; accepted December 23, 2025; available online December 23, 2025; version of record February 10, 2026; published issue March 17, 2026.*

*Computer Assisted Methods in Engineering and Science*
**33**(1): 27–49, 2026, https://doi.org/10.24423/cames.2025.1943

# Digital Tool Supporting the Documentation and Analysis of Cultural Heritage: The Case of the Analytical 3D Model of the Zamość Fortress

Michał Wac*, Bartosz Szostak

*Department of Conservation of Monuments, Faculty of Civil Engineering and Architecture, Lublin University of Technology, Lublin, Poland*

* *Corresponding Author: m.wac@pollub.pl*

This paper presents a city-scale digital documentation and analysis workflow for cultural heritage assets, demonstrated on the example of the UNESCO-listed historic centre and fortress area of Zamość (Poland). The study integrates terrestrial laser scanning (TLS) with unmanned aerial vehicle (UAV) and terrestrial photogrammetry to produce a geometrically consistent 3D dataset covering over 100 buildings and key public-space elements. The processing pipeline includes scan registration, image-based reconstruction, and cross-sensor alignment, followed by the creation of an analytical 3D model segmented by address and parcel identifiers to enable linkage with municipal datasets.

A semantic layer is implemented by assigning a structured set of building- and neighbourhood-level parameters and mapping them into building information modelling (BIM)/openBIM structures (Revit shared parameters and industry foundation classes (IFC) Property Sets), targeting a level of information adequate for conservation-oriented diagnostics and urban-scale assessments rather than detailed component-level historic building information modelling (HBIM). Geometric quality is verified using independent checkpoints and registration statistics (e.g., root mean square error (RMSE) where applicable), yielding a typical spatial agreement on the order of 4 cm to 5 cm for the integrated model in representative test areas.

The resulting environment supports multi-criteria querying and visualisation, including functional categorisation, technical condition screening (e.g., moisture-related indicators), and energy-related attributes for prioritisation at the district scale. The main contribution is a reproducible integration of multi-source survey data with an explicit semantic/BIM mapping and verifiable accuracy reporting for a heritage city context, clarifying which outputs stem from the proposed method (data integration, segmentation, semantic schema, and validation) versus the standard capabilities of the employed software.

**Keywords:** digital twin, cultural heritage documentation, 3D modelling, terrestrial laser scanning, UAV photogrammetry, BIM/IFC.

## 1. Introduction

In recent years, there has been a dynamic development of digital technologies applied to the protection of cultural heritage. Analyses indicate the growing importance of digital tools in the processes of documentation, monitoring, and conservation of historic objects [1, 2]. A prominent role is played by methods based on the integration of laser scanning, photogrammetry, and BIM modelling, which enable the precise representation and management of heritage assets [3–5].

The concept of heritage building information modelling (HBIM) has become one of the key tools in contemporary conservation practice. It allows for the creation of semantic models that combine geometric data with information on materials, damages, and previous conservation interventions [6–8, 11]. At the same time, the scan-to-BIM methodology has been evolving, serving as a bridge between spatial data acquisition and digital modelling [9]. The use of these processes contributes to the creation of complex databases that support design and conservation decision-making [1, 4, 10].

The integration of 3D scanning, photogrammetry, and BIM has been applied in numerous case studies, demonstrating its effectiveness in the documentation of heritage objects [5, 10–12]. This approach makes it possible not only to faithfully reproduce geometry but also to enrich models with semantic data and structural parameters, which significantly increases their research and practical value [1, 13]. Simultaneously, thanks to the development of visualization and augmented reality tools, such models can also be applied in education and the dissemination of heritage knowledge [9, 14].

In recent years, increasing attention has also been devoted to the concept of the digital twin, which has transitioned from industry into heritage conservation. A digital twin enables real-time monitoring, load simulations, and the analysis of structural behavior under different scenarios [15, 16]. Methodologies for implementing digital twins in the context of heritage are also being developed, taking into account the integration of geometric, material, and environmental data [17]. Complementing traditional documentation, this approach makes it possible to predict degradation processes and assess the impact of environmental factors on the longevity of heritage assets [1, 16, 18].

The study addresses digital documentation at the city scale, encompassing over 100 buildings within the historic centre of Zamość, including public spaces and selected fortification elements. The dataset integrates TLS, UAV-based photogrammetry, and terrestrial photogrammetry.

Another important aspect of heritage protection research is the focus on the intangible dimension of heritage, which allows for a more comprehensive approach to its safeguarding [19]. At the same time, knowledge management in

the context of BIM and HBIM is emphasized, leading to the creation of environments that support conservation and documentation processes [20]. The application of BIM in the documentation of historic buildings, including modernist ones, has been highlighted in international research, which points to the possibility of preserving architectural integrity while simultaneously using innovative technologies [21]. In the case of historic buildings, particular attention is also paid to issues related to Eurocodes and the requirements concerning masonry structures [22].

An important trend in the literature also includes emphasizing the significance of life cycle modelling of buildings based on BIM, enabling a holistic assessment of objects in their functional and environmental aspects [23]. At the same time, documentation and data management methods developed by international institutions, such as International Council on Monuments and Sites (ICOMOS) and United Nations Educational, Scientific and Cultural Organization (UNESCO), underline the necessity of integrating digital standards into conservation processes [24].

Research examples demonstrate that the combination of HBIM and digital twin technology may serve as the foundation for modern cultural heritage management systems. Such an approach enables predictive degradation analyses, conservation optimisation, and the integration of energy-related aspects [2, 6, 9]. Such solutions are gaining importance, particularly in the context of integrated approaches to conservation and adaptive planning [5, 17]. It is also noted that the inclusion of artificial intelligence and structural simulations in digital models may enhance their functionality and practical applicability [25]. In this context, the growing role of life cycle analysis and sustainable development aspects is also emphasized [26, 27].

Importantly, the development of digital technologies is also reflected in European regulations and research projects, which set directions for the future of conservation and the modernization of historic objects [28–30]. An example of a research initiative of considerable importance is the EASEE project, which aimed to improve the energy efficiency of multi-family buildings using modern technological solutions [31].

In summary, contemporary approaches to cultural heritage protection are increasingly based on digital tools that enable accurate documentation, analysis, and simulation of the behaviour of historic buildings and urban spaces. The integration of HBIM, scan-to-BIM, and digital twin methods into management processes constitutes a development path that not only enhances the effectiveness of heritage protection but also supports its adaptation to modern functional and environmental needs [3, 4, 12, 16, 19–24, 26].

This article fits into this research trend by focusing on the analysis of cultural heritage in the context of the city of Zamość and by demonstrating how modern

digital tools can support documentation, conservation, and adaptive processes in historic urban spaces.

The study attempts to address the research gap concerning the application of integrated digital methods (HBIM, scan-to-BIM, and digital twin) not only to the analysis and documentation of individual objects but also of entire urban complexes.

In this paper, the term 'city-scale analytical 3D model' is used to describe a geometrically consistent and semantically enriched representation of the historic urban fabric, without implying the real-time synchronisation typically associated with a full digital twin. The study focuses on scan-to-BIM integration at the district scale, targeting a level of information adequate for conservation-oriented diagnostics and urban-scale assessment rather than detailed component-level HBIM.

The aim of this article is to propose methodological and practical frameworks for documenting and analysing the historic urban fabric of Zamość, enabling the scientific systematisation and advancement of existing research in this area.

## 2. Methodology

### *2.1. Justification for the choice of location*

Zamość was selected as the subject of research due to its exceptional historical and architectural value, as well as the good availability of data and the presence of active conservation and urban planning initiatives [19, 24]. The city constitutes a coherent urban layout, enabling an analysis of the building structures and their transformations over time.

An additional advantage lies in the diversity of its building stock – ranging from monumental structures, through compact townhouse frontages, to post-industrial developments – which allows for a broad analysis of functions, technical condition, and energy potential. In the face of contemporary challenges related to the use, modernization, and energy efficiency of historic buildings, the development of a 3D model serves as a tool supporting the sustainable management of heritage resources.

The extent of the analysed area is presented in Fig. 1. The map delineates the adopted boundary of the case-study zone, covering the historic core of Zamość and the remains of the former fortress, which constituted the spatial frame for all subsequent acquisition and modelling tasks. This scope was selected to capture the complete set of key heritage structures together with their immediate urban context, while keeping the dataset size feasible for city-scale processing and semantic enrichment. The same spatial extent was also used as a consistent reference for organising datasets and linking building-level records to the 3D model.


Fig. 1. Presentation of the Old Town layout covered by our detailed study.

### *2.2. Spatial scope of the model*

The digital model covered the central part of the Zamość Fortress – the Old Town within the boundaries of the original defensive walls, with particular emphasis on the Great Market Square and the adjoining quarters [18]. The analysis encompassed approximately 100 historic buildings of diverse functions (residential, commercial, and public), supplemented by selected elements of public spaces such as the market square surface, street network, greenery, and fragments of former fortifications. This defined scope enabled to obtain a comprehensive picture of the functioning of the historic centre in urban, technical, and conservation contexts.

### *2.3. Data acquisition process: photogrammetry and laser scanning*

To develop a comprehensive 3D model of the historic centre of Zamość, an integrated spatial data acquisition methodology was applied, combining photogrammetry techniques with TLS [3, 13, 38]. Owing to their complementary properties, this approach made it possible to obtain detailed and precise geometries of heritage buildings while preserving the fidelity of architectural details [4]. The overall workflow of the applied methodology is presented in Fig. 2.

Photogrammetry was carried out both from the ground level (terrestrial photogrammetry) and from the air (aerial photogrammetry using UAVs). In total, more than 4500 digital photographs were taken, covering the entire study area – including roofs, front and rear façades, arcades, and inter-building spaces. The photographs were captured in high resolution (20 megapixels) and with approximate geolocation, facilitating the subsequent photogrammetric processing

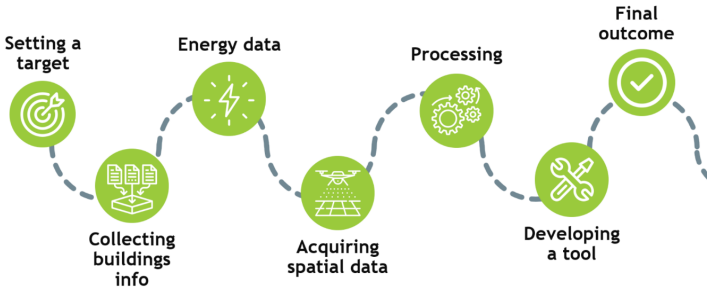


Fig. 2. Workflow of the study.

workflow. The resulting photogrammetry-based point cloud, together with the reconstructed camera positions, is shown in Fig. 3.

Fig. 3. Photogrammetry-derived point cloud and camera network (all image positions) generated in RealityCapture [33].

In parallel, more than 50 laser scans were performed from various static positions, enabling the generation of a dense point cloud representing the actual surfaces of buildings and public spaces. A geodetic-grade scanner was used, providing measurement accuracy at the level of a few millimeters and a range of up to 70 metres [24, 32]. Particular attention was devoted to the precise capture of problematic areas – such as arcade recesses, stonework details, and façade losses – which are often overlooked in standard inventory surveys. The resulting registered TLS point cloud is presented in Fig. 4.

The data acquired through both methods were processed using specialized software: FARO SCENE for the registration and merging of laser scans, and RealityCapture for generating photogrammetric models and textures. The total computation time exceeded 150 working hours, reflecting the high complexity and volume of the processed digital material [32–34].

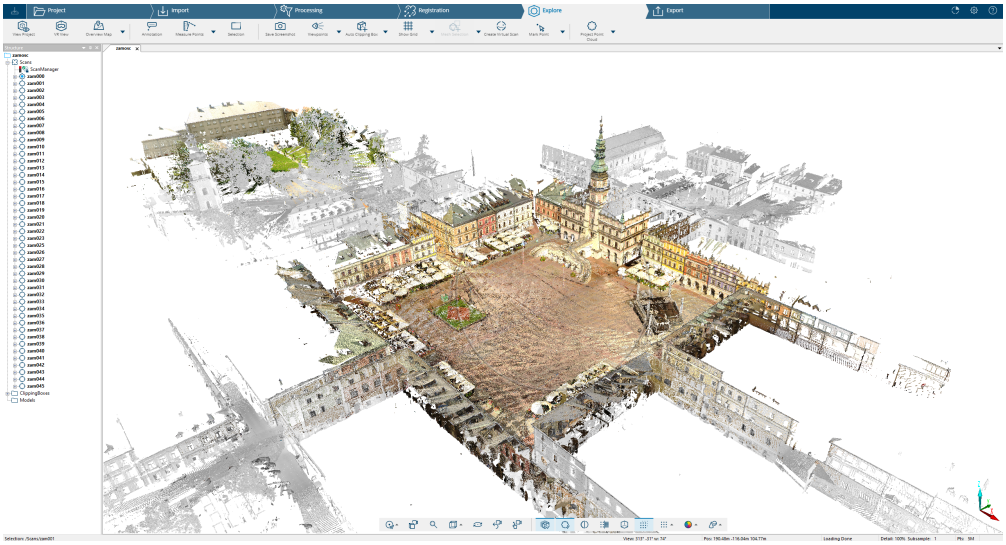

Fig. 4. TLS point cloud processed and registered in FARO SCENE [32].

A summary of the acquisition and processing parameters for photogrammetric and laser scanning data is presented in Table 1, including the number

Table 1. Summary of acquisition and processing parameters for photogrammetric and laser scanning data.

| Parameter | Photogrammetry (UAV + terrestrial) | Terrestrial Laser Scanning (TLS) | Remarks / Quality assessment |
|---|---|---|---|
| Number of images / scans | Approx. 4500 photographs | Approx. 50 scanning stations | Full coverage of the Old Town area |
| Measured surface [$m^2$] | 110 000 | 24 000 | Aerial photography covered the entire study area, whereas scanning was limited to main communication routes |
| Number of points in cloud [million] | 420 | 750 | – |
| Average point density [points/$m^2$] | Approx. 3800 | Approx. 31 250 | Combined dataset |
| Registration accuracy (RMSE) [cm/mm] | Approx. 10 cm | Avg. 10 mm | Verified against control points |
| Coverage scope | Roofs, façades, streets, courtyards | Arcades, portals, hard-to-reach zones | Complementary data |
| Software | RealityCapture | FARO SCENE | Integration in Revit/IFC |
| Total computation time [h] | Approx. 150 | Approx. 40 | Multi-core workstation |

of photographs taken, scanning stations, registration accuracy, and the main characteristics of the point clouds.

The presented comparison confirms the complementarity of the two methods – photogrammetry provided full coverage of roofs and façades, while TLS enabled high accuracy in detailed areas and hard-to-reach spaces. Combined, they allowed for the creation of a dense and precise 3D model [36]. The values in Table 1 show that the TLS dataset delivers markedly higher geometric precision (RMSE in the millimetre range) and substantially higher local point density, which is crucial for capturing fine architectural details and documenting vulnerable elements. At the same time, the photogrammetric dataset ensures complete areal coverage of the historic complex – especially roofs and upper elevations – so the integrated workflow balances completeness at the city scale with high-accuracy detail where it is most needed.

### *2.4. Data integration into the 3D model*

The next stage consisted of integrating photogrammetric and laser scanning data within a coherent 3D modelling environment [3, 9, 41]. The base geometric model was generated from the point cloud, which served as the foundation for further reconstruction of building volumes, roofs, façades, and architectural details [2, 5, 10].

The geometric quality of the integrated TLS–photogrammetry dataset was evaluated using registration statistics available from the TLS workflow and independent checkpoints/control points used for verification of alignment. The resulting spatial agreement for the integrated model was typically within 4 cm to 5 cm in representative parts of the study area, which is adequate for city-scale heritage documentation and analytical applications.

Integration of TLS and UAV/terrestrial photogrammetry data (workflow steps):

- TLS registration: individual terrestrial scans were registered into a single coherent point cloud within the TLS workflow (target-/feature-based registration), and its quality was verified using registration statistics and control points,
- photogrammetry processing (UAV + terrestrial): imagery was aligned and processed into a photogrammetry-based point cloud within the same project coordinate context, using the embedded image geolocation as an initial constraint,
- common reference frame: both datasets were brought into a unified spatial reference by applying consistent control points/checkpoints, ensuring direct comparability and minimising systematic offsets,
- dataset integration: the TLS and photogrammetric point clouds were merged into a single coherent dataset, using TLS to stabilise geometry in de-

tailed areas and photogrammetry to complement roofs and visually inaccessible zones,

– quality control: the final alignment was evaluated by independent checkpoints and by reviewing residuals and local deviations in representative areas before exporting the integrated point cloud for subsequent modelling steps.

The final point cloud contained approximately 680 million points, corresponding to an average of about 6200 points/m$^2$ across nearly 110 000 m$^2$ of the historic building complex [12]. The highest data density was obtained in the building quarters surrounding the Great Market Square, while in peripheral areas the density was lower due to a reduced number of TLS stations and limited photogrammetric coverage. As a result, the integration stage produced the raw and textured 3D models, together with the consolidated point cloud used in subsequent processing. The integrated TLS–photogrammetry result, processed in RealityCapture, is shown in Fig. 5.

Fig. 5. Integration of TLS point cloud and UAV photogrammetric model for Zamość Old Town (left: raw 3D model, centre: textured 3D model, right: point cloud) visualised in RealityCapture.

### *2.5. Segmentation of the model according to administrative divisions*

The developed 3D model was divided into logical segments corresponding to building quarters and individual structures, in line with the existing administrative and functional divisions. Each building was assigned a unique identifier and linked to a specific spatial unit (street, address number, cadastral parcel) [18, 21, 35]. This allowed the model to be connected with data from

municipal resources, including building registries, heritage registers, and energy consumption records [6, 14].

Such segmentation enables end users to easily filter, select, and compare objects in both spatial and technical contexts. For example, it becomes possible to identify all buildings connected to the district heating network, compare their energy demand and thermal insulation condition, and then visualize the results on a 3D map in real time [35]. An overview graphic of this stage is provided in Fig. 6.

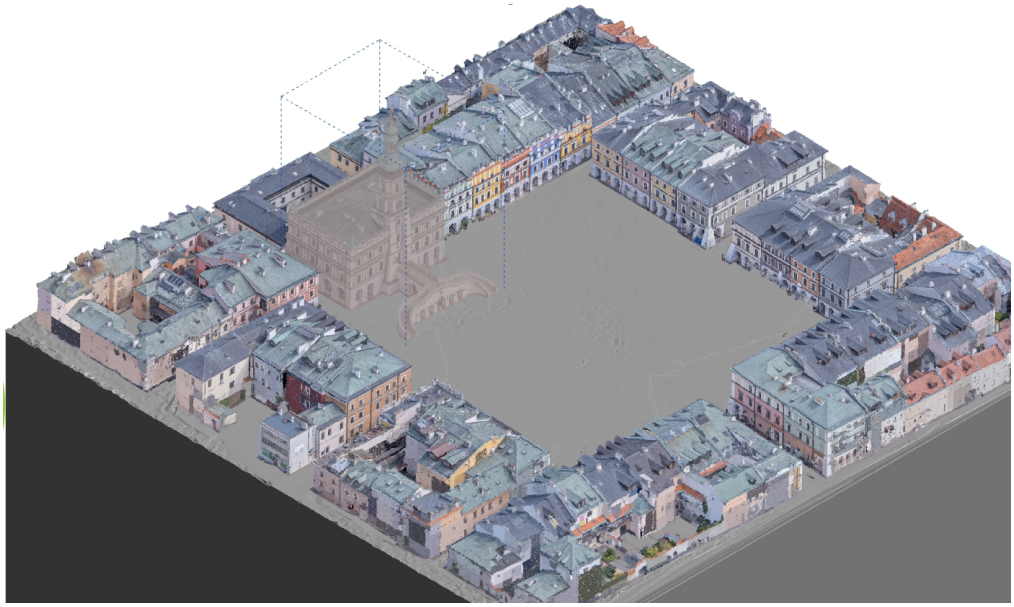

Fig. 6. Example of object selection in the segmented model – individual building elements can be selected independently, rather than selecting the entire model as a single object.

The introduction of the administrative layer also extends the model's applications to spatial planning, urban analyses, public consultations, and educational activities. Moreover, the segmentation establishes a one-to-one mapping between each geometric segment and its semantic record via a unique building identifier, enabling automated linking of spreadsheet/database attributes to BIM objects (Revit/IFC) in subsequent steps.

The spatial data segmented according to administrative divisions were imported into a BIM environment, using software such as Autodesk Revit and data interoperability tools (including CloudCompare and IFC Viewer). At this stage, semantic information was assigned to each model element – both geometric (e.g., façade area, number of floors) and functional-technical (e.g., heating type, roof condition, thermal insulation).

The entire dataset was saved in IFC format, ensuring compatibility with other IT systems and enabling further processing of the model in external analytical environments [14].

Each geometric segment created during segmentation was assigned a unique BuildingID/ObjectID, which served as the primary key linking geometry to the corresponding row in the attribute table. This established a one-to-one mapping between model objects and semantic records, enabling automated parameter assignment and reducing manual errors.

### *2.6. Preparation of descriptive data and preliminary analysis*

In parallel with the development of the geometric model, a process was carried out to collect descriptive (semantic) data for all buildings included in the model [6, 7, 20]. This information was gathered from various sources, including:

- resources of the Department of Investment and Development of the City of Zamość,
- municipal building registries,
- geodetic and urban planning documentation,
- materials prepared by conservation and technical units.

The collected dataset covered more than 100 buildings, with each assigned a set of over 10 descriptive parameters, including:

- address and functional use,
- building footprint and number of storeys,
- technical condition of façades, roofs, and joinery,
- type of heating system and heat source,
- level of insulation of external partitions (walls, roof),
- presence and type of renewable energy sources,
- estimated annual energy demand.

The data were standardised and entered into spreadsheets, and then imported into the BIM modelling environment [21, 34]. By assigning unique identifiers to the buildings (consistent with the Revit/IFC system), it was possible to automatically link the data to the corresponding objects in the model. The entire process was carried out in a way that enables future data synchronisation – for example, in the event of updates [37]. An overview graphic of this stage is provided in Fig. 7.

In addition, a preliminary analysis of the collected data was carried out, which made it possible to determine the typology of buildings, identify structures in poor technical condition, and highlight special cases (e.g., buildings not connected to the district heating network, or those using heat pumps, etc.) [23].

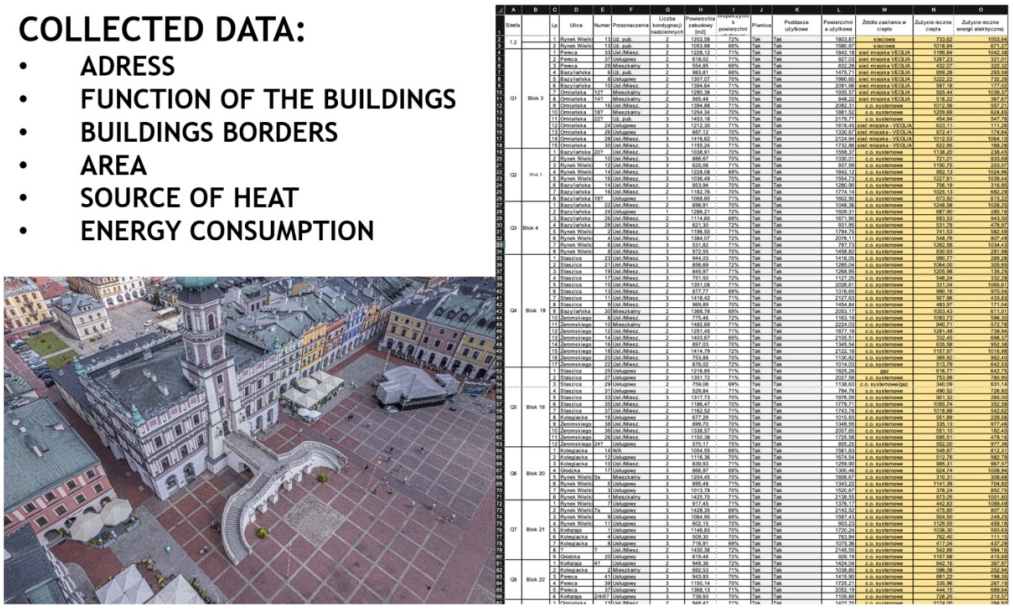


Fig. 7. Data standardisation process illustrated by a fragment of the semantic attribute table shown in Microsoft Excel (XLSX/CSV table).

This analysis served as the starting point for the further classification of objects into appropriate conservation and energy-related categories.

Semantic attributes were stored in structured spreadsheets (XLSX/CSV) following a 'one record–one building' rule. The dataset was standardised using controlled vocabularies, predefined units, and value ranges to reduce ambiguity and ensure consistent querying. Prior to BIM import, the tables were validated for completeness, data types, and uniqueness of identifiers (missing values, duplicates, and out-of-range entries were flagged and corrected).

### *2.7. Process structure and workflow organization*

The overall methodology was structured as a coherent, iterative workflow consisting of seven consecutive stages, consistent with the scheme presented in Fig. 2. The stages were implemented with feedback loops between data acquisition, processing, and validation, to ensure both geometric reliability and semantic consistency of the analytical model [6, 9, 14]:

– setting a target (Subsec. 2.1) – defining the intended use of the model (heritage documentation, conservation-oriented diagnostics, and urban/energy-related analyses), establishing the spatial extent and level of detail, and formulating the key outputs expected from the digital twin [15, 17],

- collecting building information (Subsec. 2.6) – compiling the base inventory of buildings and public-space elements included in the study, assigning unique identifiers, and gathering core administrative and descriptive attributes required for subsequent integration and database structuring [6, 20],
- energy data (Subsec. 2.6) – collecting and standardising energy-related attributes (e.g., heating type, estimated energy demand, insulation status, and related indicators) as a dedicated subset of the semantic dataset, using unified scales and controlled vocabularies to enable subsequent filtering and comparative analyses [27, 29],
- acquiring spatial data (Subsec. 2.3) – performing UAV and terrestrial photogrammetry operations and terrestrial laser scanning to capture complementary spatial datasets covering roofs, façades, streets, courtyards, and difficult-to-reach architectural details, while maintaining consistent referencing of the acquired material [11, 32, 38],
- processing (Subsec. 2.4) – registering and merging TLS scans, processing photogrammetric imagery, integrating both sources into a coherent spatial dataset, and generating the base geometric representation used for further reconstruction, segmentation, and preparation for information enrichment [3, 10, 36],
- developing a tool (Subsec. 3.3) – importing the segmented model into the BIM environment, assigning semantic information through dedicated parameters linked by unique identifiers, exporting structured outputs (e.g., IFC), and implementing an interactive digital twin interface enabling attribute-based visualisation, filtering, and reporting [1, 6, 14],
- final outcome (Subsec. 4.1) – obtaining an analytical, city-scale 3D model integrating geometry and standardised descriptive/energy data, prepared for multi-criteria assessments and future updates, with documented procedures supporting reproducibility and transferability to other historic urban contexts [17, 23, 25].

### *2.8. Methodological conclusions*

The adopted approach proved both effective and scalable, allowing for the development of a highly detailed, segmented urban model that can be expanded and updated in subsequent stages [1, 9]. The key success factors included:

- the use of complementary technologies (laser scanning + photogrammetry) [5],
- the application of BIM and IFC standards as a common data integration language,

– precise coordination of geometric and descriptive data,
– the ability to perform multi-criteria analyses of diverse object attributes.

The developed methodology can serve as a model for other cities and research teams engaged in the documentation and analysis of cultural heritage in spatial terms. In the next stages, the model's application is planned to be extended with additional diagnostic and analytical functionalities, which will be discussed in later sections of the article [17].

## 3. Semantic data management

### *3.1. Categories of information assigned to model segments*

One of the key elements in building the analytical model of the Zamość Fortress was the development of a semantic data structure, i.e., descriptive information linked to the geometric representations of buildings [1, 20]. These data serve as the basis for conducting technical, energy-related, functional, and conservation analyses [11].

For each building in the model, a standardised set of parameters – organised into logical thematic categories – was assigned, defined based on ISO 19650 principles and structured according to IFC4 Property Set logic.

Identification and location:
– address (street, number),
– cadastral parcel number,
– Revit/IFC identifier.

Functional and usage-related:
– main building function (residential, commercial, institutional),
– attic accessibility (usable/non-usable),
– number of above-ground and underground floors.

Geometric parameters:
– building footprint,
– usable floor area (if available),
– volume (for selected objects).

Technical condition:
– assessment of façade, roof, and window/door joinery condition,
– moisture level in basements,
– technical condition of sanitary installations.

Energy and environmental characteristics:
– type of heating (district heating, gas, biomass, heat pump, none),
– estimated annual energy demand [kWh/m$^2$/year],

– level of wall and roof insulation,
– presence of renewable energy sources (PV, collectors, heat pumps).

The parameters were defined with explicit units and data types, using consistent naming conventions and controlled vocabularies where applicable, to ensure validation, comparability, and seamless mapping to IFC4 Property Sets for interoperable analysis.

This set of attributes was standardised in the form of input data tables (spreadsheets in CSV/XLSX format) and subsequently linked to the 3D models through unique identifiers assigned to each object. The data were categorised in a way that enabled easy filtering and grouping of buildings according to any criterion (e.g., all residential buildings with non-modernised roofs and gas heating) [23].

### *3.2. Database structure*

For the purposes of the model, a flat relational database was developed, based on a 'one row – one building' scheme, with columns corresponding to descriptive parameters [21]. The database schema was adapted to the data import format for the BIM environment (Autodesk Revit) and for further analysis in external tools (e.g., CloudCompare, CellBIM).

Selected features of the data structure include:

– all fields were standardised (e.g., technical condition rating scales from 1 to 5, functional codes consistent with the national statistical classification – Główny Urząd Statystyczny (GUS)) [34],
– data types were clearly assigned (text, integer, floating-point number, Boolean value),
– consistency control was introduced (range validation, no duplicates, uniqueness of identifiers) [34].

An illustrative view of the implemented database schema and example records is shown in Fig. 8.

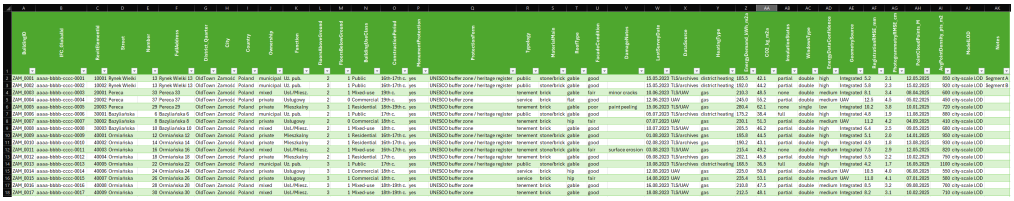

FIG. 8. Example of the building-attribute database used in the workflow (Subsec. 3.2), implemented as a structured Microsoft Excel table following the 'one record–one building' rule, with unique BuildingID and BIM linkage keys (IFC_GlobalId, RevitElementId), and grouped fields covering administrative, heritage, energy, and geometry/quality parameters for subsequent mapping to BIM objects and IFC Property Sets.

The data are stored in a way that enables updating – changes in the database can be automatically synchronised with the 3D model via assigned IDs and corresponding family parameters (Revit Families) [20, 37].

### *3.3. Integration of data with the 3D model*

In Autodesk Revit, semantic information was implemented as dedicated project/shared parameters, grouped into thematic sets (administrative, heritage, and energy-related). Parameter values were populated from the validated tables using the BuildingID/ObjectID key (semi-automated assignment), ensuring that each BIM object inherits the correct attributes. The enriched model was exported to IFC4, where the attributes were preserved as Property Sets linked to the corresponding geometric elements, enabling consistent use in external analytical environments.

The integration of semantic data with the 3D model was carried out in two stages:

1. Import into the BIM environment (Autodesk Revit)
   The spatial model was enriched with descriptive data through dedicated project parameters. Each object was assigned fields containing information from the input table. An overview illustration of this stage is presented in Fig. 9.
2. Synchronisation with analytical tools (e.g., CellBIM, CloudCompare)
   Data export was carried out in IFC4 format, compliant with the international standard for building information exchange [34]. This enabled the use of the model in external environments (including CellBIM for

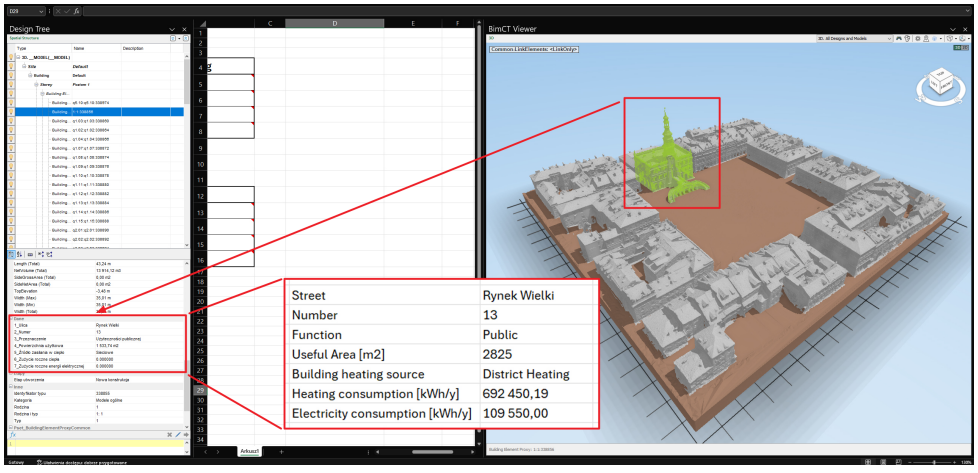


Fig. 9. Integration of data with the 3D Model. The IFC model is presented in Microsoft Excel with the CellBIM add-in, illustrating how object-level attributes are accessible as Property Sets for analysis and verification.

data analysis and CloudCompare for 3D data visualisation) [18]. In these environments, the data were read as Property Sets linked to geometric objects [34]. To demonstrate the effect of semantic enrichment, a sample building object is shown in Fig. 10 with its assigned parameter set. The same attributes are readable after IFC export as Property Sets, enabling attribute-based filtering and inspection in external tools.

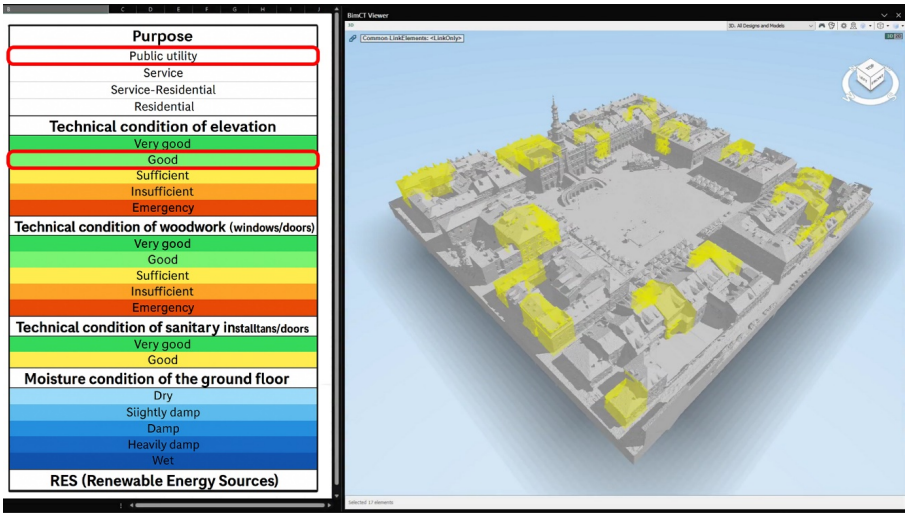


Fig. 10. Synchronisation of the enriched IFC4 model with external analytical tools for querying and visualisation. The figure presents an attribute-based inspection of Property Sets using tools such as CellBIM (data analysis), supporting filtering and verification of semantic information against the geometry.

The functionality of creating colour-coded attribute maps was also utilised – for example, to graphically represent energy consumption levels, insulation quality, or the condition of building elements [40]. This facilitates visual analysis and the identification of problematic objects within the historic urban fabric.

## 4. Results and conclusions

### *4.1. Assessment of the effectiveness of the approach*

The effectiveness of the proposed workflow was evaluated using four criteria: geometric accuracy and alignment of the integrated spatial datasets, coverage and scalability at the level of the historic city centre, semantic completeness and consistency of the attribute database, and interoperability and usability of the enriched model in external analytical environments. The resulting analytical model covers more than 100 buildings within the historic centre and combines city-scale geometry with standardised descriptive information [34, 36, 41].

From a technical perspective, the following evidence was obtained:

- Geometric accuracy and alignment: the quality of the integrated TLS–photogrammetry dataset was verified using registration statistics from the TLS workflow and independent checkpoints/control points. In representative parts of the study area, the resultant spatial agreement after integration was typically within 4 cm to 5 cm, which is suitable for city-scale heritage documentation and comparative analyses [36];
- Coverage and scalability: the acquisition strategy ensured complementary coverage of roofs, façades, streets, courtyards, and hard-to-reach zones by combining UAV/terrestrial photogrammetry with terrestrial laser scanning, enabling a coherent representation of the historic urban fabric at the scale of the entire pilot area [41];
- Semantic completeness and consistency: a flat 'one row – one building' database was implemented with standardised fields, controlled vocabularies and range validation, and unique identifiers used as keys for automated linking between geometry and attributes. In the presented implementation, each building was described by a consistent core set of parameters (e.g., function, typology, condition and selected energy indicators), enabling repeatable querying and future updates without breaking the ID mapping [34];
- Interoperability and usability: the enriched model was exported in IFC4 and verified by reading the assigned Property Sets in external environments (e.g., CellBIM for attribute inspection and CloudCompare for 3D visualization). In addition, the interactive tool was tested on the 100-building dataset, supporting object-level selection and attribute-based exploration in a web-based context [34, 41].

Overall, the results demonstrate that the integration of heterogeneous sources (spatial surveys and administrative/heritage/energy attributes) can be implemented in a reproducible way, enabling practical heritage-management use cases such as condition screening, multi-criteria comparisons, and identification of modernisation potential at the scale of a historic town centre [34, 41].

### *4.2. Examples of applications in urban analysis*

Based on the developed model, a series of thematic analyses were conducted, the results of which can be treated as direct indicators of the tool's usefulness. Selected examples include:

- Functional analysis revealed that a significant share of service-oriented buildings is concentrated around the Great Market Square, with a tendency to disperse toward the eastern quarters. This finding may serve

as a basis for the revitalisation of residential buildings and their adaptation to commercial functions in line with conservation guidelines [39];
- Technical condition analysis enabled the identification of buildings requiring urgent conservation interventions (e.g., structures with leaky roofing or visible damage to joinery or façades). Such information can support the activities of municipal heritage protection services [11, 22];
- Energy analysis made it possible to identify buildings with the highest estimated energy demand (above 250 kWh/m$^2$/year), mainly in structures with unused attics, outdated heating systems, or a lack of partition insulation [26, 29, 31]. These results can serve as a foundation for planning thermal modernisation actions.

All of the above data were presented in real time within the interactive environment, with options for exporting reports and filtering results according to selected criteria.

### *4.3. Potential for tool development*

The developed digital model and analytical tool represent only the first stage of a broader system supporting cultural heritage management in historic cities [8, 17]. In subsequent stages, the following development directions are possible:
- integration with temporal data – introducing change histories for each building, enabling the analysis of urban space transformations over time (e.g., renovations, functional changes, structural modifications) [37],
- real-time updating – implementing a synchronisation system with municipal cadastral databases (e.g., GESUT, EGiB, MPZP), allowing for the automatic refreshing of the model and descriptive data [35],
- extension to additional city areas – the scalability of the method makes it applicable not only within the boundaries of the Old Town but also in adjacent districts, including 19th- and 20th-century heritage sites [41],
- introduction of a participatory layer – enabling residents, investors, or researchers to add annotations and submit comments on individual objects, while maintaining expert oversight and content validation.

## 5. Final summary

The conducted research confirmed that modern digital documentation technologies can be effectively used not only for inventory purposes but, above all, as analytical tools supporting rational and sustainable cultural heritage management. The case of the Zamość Fortress demonstrated that it is possible to reconcile documentation precision with practical applications in planning, energy

management, conservation, and education. The developed model may provide a reference model for other cities and institutions seeking to implement digital twins in heritage protection.

## Acknowledgements

The research was carried out within the framework of the ZEB4ZEN – Zero Energy Buildings for Zero Energy Neighbourhoods project, co-funded by the European Union under the Interreg programme.

## References

1. López F.J., Lerones P.M., Llamas J., Gómez-García-Bermejo J., Zalama E., A review of heritage building information modelling (H-BIM), *Multimodal Technologies and Interaction*, **2**(2): 21, 2018, https://doi.org/10.3390/mti2020021.
2. Biagini C., Capone P., Donato V., Facchini N., Towards the BIM implementation for historical building restoration sites, *Automation in Construction*, **71**: 74–86, 2016, https://doi.org/10.1016/j.autcon.2016.03.003.
3. Alshawabkeh Y., Baik A., Miky Y., Integration of laser scanner and photogrammetry for heritage BIM enhancement, *ISPRS International Journal of Geo-Information*, **10**(5): 316, 2021, https://doi.org/10.3390/ijgi10050316.
4. Masciotta M.G., Sanchez-Aparicio L.J., Oliveira D.V., González-Aguilera D., Integration of laser scanning technologies and 360° photography for the digital documentation and management of cultural heritage buildings, *International Journal of Architectural Heritage*, **17**(1): 56–75, 2023, https://doi.org/10.1080/15583058.2022.2069062.
5. Andriasyan M., Moyano J., Nieto-Julián J.E., Antón D., From point cloud data to building information modelling: An automatic parametric workflow for heritage, *Remote Sensing*, **12**(7): 1094, 2020, https://doi.org/10.3390/rs12071094.
6. Jordan-Palomar I., Tzortzopoulos P., García-Valldecabres J., Pellicer E., Protocol to manage heritage-building interventions using heritage building information modelling (HBIM), *Sustainability*, **10**(4): 908, 2018, https://doi.org/10.3390/su10040908.
7. Sztwiertnia D., Ochałek A., Tama A., Lewińska P., HBIM (heritage building information modell) of the Wang Stave Church in Karpacz – Case study, *International Journal of Architectural Heritage*, **15**(5): 713–727, 2019, https://doi.org/10.1080/15583058.2019.1645238.
8. Chen L., Dai C., Zhou M., Lu J., Development and application of an HBIM method for timber structures integrated with digital technologies, *npj Heritage Science*, **13**: 381, 2025, https://doi.org/10.1038/s40494-025-01925-2.
9. Rocha G., Mateus L., Fernandez J.H., Ferreira V., A scan-to-BIM methodology applied to heritage buildings, *Heritage*, **3**(1): 47–67, 2020, https://doi.org/10.3390/heritage3010004.
10. Crisan A., Pepe M., Costantino D., Herban S., From 3D point cloud to an intelligent model set for cultural heritage conservation, *Heritage*, **7**(3): 1419–1437, 2024, https://doi.org/10.3390/heritage7030068.

11. Szostak B., Wac M., The use of digital technologies in assessing the technical condition of historic structures, *Budownictwo i Architektura*, **23**(4): 151–172, 2024, https://doi.org/10.35784/bud-arch.6669.

12. Barazzetti L., Banfi F., Brumana R., Gusmeroli G., Previtali M., Schiantarelli G., Cloud-to-BIM-to-FEM: Structural simulation with accurate historic BIM from laser scans, *Simulation Modelling Practice and Theory*, **57**: 71–87, 2015, https://doi.org/10.1016/j.simpat.2015.06.004.

13. Dore C., Murphy M., McCarthy S., Brechin F., Casidy C., Dirix E., Structural simulations and conservation analysis – historic building information model (HBIM), *ISPRS International Archives of the Photogrammetry, Remote Sensing and Spatial Information Sciences*, **XL-5/W4**: 351–357, 2015, https://doi.org/10.5194/isprsarchives-XL-5-W4-351-2015.

14. Oostwegel L.J.N., Jaud Š., Muhič S., Malovrh Rebec K., Digitalization of culturally significant buildings: ensuring high-quality data exchanges in the heritage domain using OpenBIM, *Heritage Science*, **10**: 10, 2022, https://doi.org/10.1186/s40494-021-00640-y.

15. Funari M.F., Hajjat A.E., Masciotta M.G., Oliveira D.V., Lourenço P.B., A parametric scan-to-FEM framework for the digital twin generation of historic masonry structures, *Sustainability*, **13**(19): 11088, 2021, https://doi.org/10.3390/su131911088.

16. Vuoto A., Funari M.F., Lourenço P.B., Shaping digital twin concept for built cultural heritage conservation: A systematic literature review, *International Journal of Architectural Heritage*, **18**(11): 1762–1795, 2024, https://doi.org/10.1080/15583058.2023.2258084.

17. Noronha Pinto de Oliveira e Sousa M., Correa F.R., Towards digital twins for heritage buildings: A workflow proposal, *International Journal of Architectural Computing*, **21**(4): 712–729, 2023, https://doi.org/10.1177/1478077123116822.

18. Pepe M., Palumbo D., Dewedar A.K.H., Spacone E., Toward to combination of GIS-HBIM models for multiscale spatial information about an historic center, *Heritage*, **7**(12): 6966–6980, 2024, https://doi.org/10.3390/heritage7120322.

19. Vecco M., A definition of cultural heritage: From the tangible to the intangible, *Journal of Cultural Heritage*, **11**(3): 321–324, 2010, https://doi.org/10.1016/j.culher.2010.01.006.

20. Acierno M., Cursi S., Simeone D., Fiorani D., Architectural heritage knowledge modelling: An ontology-based framework for conservation process, *Journal of Cultural Heritage*, **24**: 124–133, 2017, https://doi.org/10.1016/j.culher.2016.09.010.

21. Penttilä H., Rajala M., Freese S., Building information modelling of modern historic buildings, in: *Proceedings of the 25th eCAADe Conference on Predicting the Future*, pp. 607–613, Frankfurt am Main, Germany, 26–29 September, 2007, https://doi.org/10.52842/conf.ecaade.2007.607.

22. Tomaževič M., Lutman M., Heritage masonry buildings in urban settlements and the requirements of Eurocodes: Experience of Slovenia, *International Journal of Architectural Heritage*, **1**(1): 108–130, 2007, https://doi.org/10.1080/15583050601126186.

23. Gursel I., Sariyildiz S., Akin Ö., Stouffs R., Modelling and visualization of lifecycle building performance assessment, *Advanced Engineering Informatics*, **23**(4): 396–417, 2009, https://doi.org/10.1016/j.aei.2009.06.010.

24. Letellier R., Eppich R. [Eds.], *Recording, Documentation and Information Management for the Conservation of Heritage Places*, Routledge, Abingdon, UK, 2015.

25. Battina S., Jaganathan S., AI and digital twin applications in 3D information models for heritage buildings: A systematic review, *International Journal of Engineering and Technology Management Sciences*, **7**(3): 122–131, 2023, https://doi.org/10.46647/ijetms.2023.v07i03.017.

26. Najjar M., Figueiredo K., Palumbo M., Haddad A., Integration of BIM and LCA: Evaluating the environmental impacts of building materials at an early stage of designing a typical office building, *Journal of Building Engineering*, **14**: 115–126, 2017, https://doi.org/10.1016/j.jobe.2017.10.005.

27. Eleftheriadis S., Mumovic D., Greening P., Life cycle energy efficiency in building structures: A review of current developments and future outlooks based on BIM capabilities, *Renewable and Sustainable Energy Reviews*, **67**(C): 811–825, 2017, https://doi.org/10.1016/j.rser.2016.09.028.

28. EU Directive 2018/844/EU, Energy Performance of Buildings, Official Journal of the European Union, 2018.

29. Directive of the European Parliament and of the Council, On the energy performance of buildings, Official Journal of the European Union, 2021.

30. Ministry of Economic Development, Ministry of the Environment and Protection of Natural Resources and the Sea, Integrated national energy and climate plan, European Commission, 2020.

31. EASEE Project, Envelope approach to improve sustainability and energy efficiency in existing multi-storey multi-owner residential buildings, CORDIS, 2016.

32. FARO Technologies, User manual for SCENE, online: https://knowledge.faro.com/Software/FARO_SCENE/SCENE/User_Manual_for_SCENE [access: 23.09.2025].

33. Capturing Reality, RealityCapture – Documentation and Manual, Epic Games, online: https://dev.epicgames.com/community/learning/knowledge-base/R85v/realityscan-help-realitycapture-documentation-and-manual [access: 23.09.2025].

34. Argasiński K., Kuroczyński P., Preservation through digitization – Standardization in documentation of build cultural heritage using capturing reality techniques and heritage/historic BIM methodology, *The International Archives of the Photogrammetry, Remote Sensing and Spatial Information Sciences*, **XLVIII-M-2**: 87–94, 2023, https://doi.org/10.5194/isprs-archives-XLVIII-M-2-2023-87-2023.

35. Stylianidis E., Evangelidis K., Vital R., Dafiotis P., Sylaiou S., 3D documentation and visualization of cultural heritage buildings through the application of geospatial technologies, *Heritage*, **5**(4): 2818–2832, 2022, https://doi.org/10.3390/heritage5040146.

36. Jo Y.H., Park J.H., Hong E., Han W., Three-dimensional digital documentation and accuracy analysis of the Choijin Lama Temple in Mongolia, *Journal of Conservation Science*, **36**(4): 264–274, 2020, https://doi.org/10.12654/JCS.2020.36.4.04.

37. Kong X., Monitoring time-varying changes of historic structures through photogrammetry-driven digital twinning, *The International Archives of the Photogrammetry, Remote Sensing and Spatial Information Sciences*, **XLVIII-2**: 181–186, 2024, https://doi.org/10.5194/isprs-archives-XLVIII-2-2024-181-2024.

38. Fidan Ş., Ulvi A., Yiğit A.Y., Hamal S.N.G., Yakar M., Combination of terrestrial laser scanning and unmanned aerial vehicle photogrammetry for heritage building information modelling: A case study of Tarsus St. Paul Church, *Photogrammetric Engineering and Remote Sensing*, **89**(12): 753–760, 2023, https://doi.org/10.14358/PERS.23-00031R2.

39. Szostak B., Wac M., Historic crypts of the Church of the Exaltation of the Holy Cross in Łuków – Challenges preceding adaptation, *Zeszyty Naukowe Politechniki Poznańskiej. Architektura, Urbanistyka, Architektura Wnętrz*, **2024**(20): 51–75, 2024, https://doi.org/10.21008/j.2658-2619.2024.20.4.

40. Aricò M., Dardanelli G., La Guardia M., Lo Brutto M., Three-dimensional documentation and virtual web navigation system for the indoor and outdoor exploration of a complex cultural heritage site, *Electronics*, **13**(14): 2833, 2024, https://doi.org/10.3390/electronics13142833.

41. Konstantakis M. *et al.*, An improved approach for generating digital twins of cultural spaces through the integration of photogrammetry and laser scanning technologies, *Digital*, **4**(1): 215–231, 2024, https://doi.org/10.3390/digital4010011.

*Received September 28, 2025; revised December 19, 2025; accepted December 22, 2025; available online December 23, 2025; version of record January 22, 2026; published issue March 17, 2026.*

*Computer Assisted Methods in Engineering and Science*
**33**(1): 51–68, 2026, https://doi.org/10.24423/cames.2025.1936

# The Impact of Point Cloud Simplification on the Accuracy of the Viewshed

Jerzy Orlof*, Adrian Widłak

*Faculty of Computer Science and Telecommunications, Cracow University of Technology, Cracow, Poland*

* *Corresponding Author: jerzy.orlof@pk.edu.pl*

Contemporary visibility analyses, particularly relevant in environmental and landscape studies, require the processing of very large datasets derived from point clouds. While such data provide high accuracy, they also involve substantial computational demands and long processing times, which limit their practical applicability. This article presents a detailed analysis of the impact of point cloud simplification on the accuracy of viewshed. The viewshed diagrams were generated using the ray tracing method, and the analysis included an evaluation of discrepancies between results obtained from simplified datasets and reference outcomes based on the complete, unprocessed dataset. In addition, the computation time required to generate viewshed under different levels of simplification was investigated. The findings made it possible to identify the maximum acceptable levels of simplification as well as the potential computational gains in terms of the number of processed points. The results demonstrate that properly selected simplification levels can significantly enhance the efficiency of ray tracing-based visibility analyses while preserving their practical reliability.

**Keywords:** visibility analysis, viewshed, point cloud, geometric accuracy, 3D data processing, spatial analysis.



## 1. Introduction

In contemporary expert assessments, two factors are of primary importance: the precision of analyses and the time required for their execution. Engineers face the challenge of achieving the highest possible accuracy of results within the shortest feasible time. This problem concerns various fields of analysis, including visibility assessment [1]. Determining visibility requires a range of analyses, such as three-dimensional (3D) models, photographic documentation, or visibility diagrams [2]. Visibility analysis based on a viewshed diagram, constructed

from a terrain model generated using point clouds [3], demands substantial computational resources [4] in order to fully exploit the accuracy provided by the point cloud. Unfortunately, the volume of data is so large that the analysis time becomes very long and, in some cases, impossible to achieve within reasonable limits [5]. Time is therefore a critical factor, as the generation of a single viewshed has an exponential effect on the production of a visibility map, which may consist of hundreds or even thousands of diagrams. Studies on the visual protection surface (VPS) method have shown that the resolution of 3D models and the density of viewpoint sampling significantly influence the accuracy of viewshed analysis results, while computational costs increase exponentially with increasing data detail [6]. This highlights the need for a systematic evaluation of the impact of point cloud simplification on the reliability of viewshed analyses.

To accelerate the generation of viewshed maps, various point cloud simplification methods are applied [7]. Several approaches to point cloud simplification can be distinguished. One group includes methods based on hierarchical clustering, while others simplify data through the sampling of characteristic points (feature-based sampling) [8, 9]. These methods rely on advanced, often proprietary, computational models.

There are also random approaches [10], which are relatively simple and widely used in various applications. Their drawback, however, is the lack of determinism – the results may vary with each execution of the algorithm.

It is worth noting that many of the above methods are not widely available: point cloud processing software often does not implement them, or the generated results are not reproducible.

The most commonly used approaches, implemented for instance in AutoCAD and CloudCompare, are based on reducing the density of the point cloud according to a specified minimum distance $\delta$ between points [11]. Formally, this process can be expressed as selecting a subset $P' \subseteq P$ from the original point set $P = \{p_1, p_2, ..., p_n\}$ such that:

$$\min_{q \in P'} \|p_i - q\| \geq \delta.$$

More advanced approaches rely on local curvature analysis. Other methods employ information entropy.

In this article, the method of reducing point density according to a specified minimum distance between points was employed as the primary technique for simplifying the input data. Nevertheless, excessive simplification can introduce distortions and, consequently, lead to incorrect analytical results, which is unacceptable. For this reason, the simplification process was subjected to a detailed two-stage examination.

The first parameter of primary importance was accuracy. Since the accuracy of results decreases as the data are simplified, the study investigated the minimum level of accuracy that does not cause significant distortions. The second critical aspect considered was computation time. Here, the analysis focused on the time required to generate viewshed diagrams at different simplification levels, with the aim of identifying the shortest processing time corresponding to the minimum acceptable accuracy of the viewsheds.

## 2. Materials and methods

### *2.1. Point cloud*

For the analysis, publicly available LiDAR data from geoportal.gov.pl were used (Fig. 1), derived from the national airborne laser scanning resource [12, 13]. The dataset corresponds to a digital elevation model (DEM) covering the area marked M-34-64-D-d-4-1-2-1 in Kraków, with an average density of 12 points/m$^2$. The area was scanned in 2023. Point elevations range from $h_{\min} = 161.69$ m to $h_{\max} = 334.12$ m above sea level, resulting in a total elevation difference of $\Delta h = 172.43$ m. Recorded slope values vary from 0° up to an extreme maximum of 88°. The selected area is characterized by diverse landforms, including a prominent hill, flat surfaces, urban structures, and forested terrain, as well as faults indicated by very steep slopes. This heterogeneity allows for the evaluation of simplification-induced errors across different types of topographic conditions.

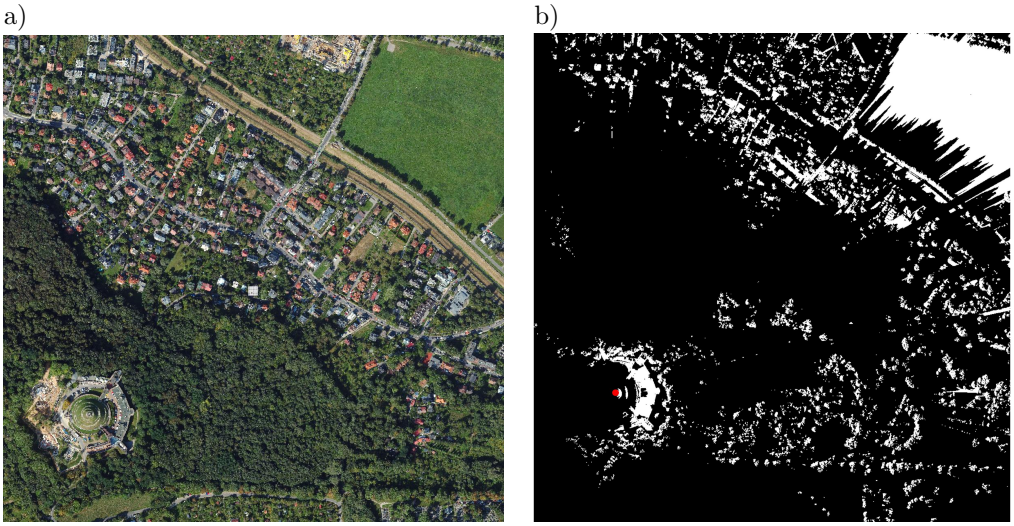


Fig. 1. Comparison of the point cloud (a) and the resulting viewshed (b). The observation point is marked with a red dot.

The point cloud was acquired using airborne LiDAR, where $x$, $y$ coordinates were determined from GPS positioning and the $z$ coordinate was calculated from the return time of a laser pulse emitted vertically toward the ground [14–16]. Each point is represented by spatial coordinates ($x$, $y$, $z$) and additional attributes such as RGB color values or point classification [17]. The dataset used in this study was provided in LAZ format [18], which allows efficient compression of large point clouds while preserving their accuracy.

### *2.2. Viewshed vs. visibility analysis*

The term viewshed, introduced several decades ago by Tandy [19] and later developed by Benedikt [20], can be defined as a graphical representation of visible and non-visible areas from a specific observation point with coordinates ($x$, $y$, $z$) [1] (Fig. 1b). Such a diagram allows for the straightforward identification of areas obscured by terrain or other structures and those visible from the observer's position. In computational applications, viewshed analysis is typically performed using line-of-sight calculations based on digital terrain models or 3D spatial representations. Viewshed diagrams are highly versatile; for instance, they are widely used in spatial planning to evaluate whether new constructions interfere with the surrounding environment or landscape. They are also applied in tourism development, where viewsheds help identify optimal viewpoints along planned trails, thereby enhancing their attractiveness to visitors.

In contrast, visibility analysis (also referred to as visibility mapping) is a broader concept. A visibility map [2] can be understood as a composite structure consisting of multiple viewsheds generated from different observation points. The distribution and density of observation points strongly influence the resulting visibility map, affecting both its spatial resolution and analytical reliability. This integrated visualization enables the identification of panoramic routes and the assessment of cumulative visibility across an area. As a result, visibility analysis provides a more comprehensive perspective, supporting urban design, landscape management, and the development of recreational infrastructure.

### *2.3. Generating viewsheds based on point clouds*

In order to generate a viewshed [1], different types of elevation data representations can be used. One approach involves creating a surface from the point cloud, for example in the form of a regular grid or a triangulated irregular network (TIN) [4] (Fig. 2). The TIN surface, based on the Delaunay triangulation algorithm, provides high precision and is frequently employed in visibility studies. Alternatively, many popular GIS tools, such as QGIS, allow viewsheds to be generated directly from digital elevation models (DEMs) or digital terrain

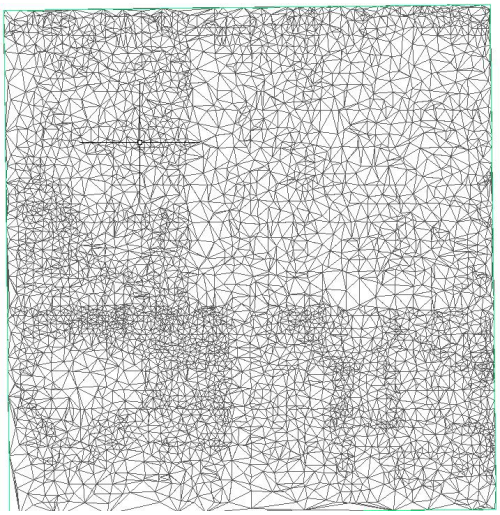

Fig. 2. Tin surface for the area analysed in the study.

models (DTMs/DSMs) in raster form – but viewshed charts are not as highly accurate as those based on point clouds.

Regardless of the chosen method, the process involves placing an observation point at a given location and analyzing terrain obstruction along the line of sight. The result is a graphical representation of visible and non-visible areas, typically encoded in binary form (e.g., visible areas shown in white and non-visible areas in black).

### *2.4. Computing machine parameters*

The calculations were executed on a high-performance workstation featuring an Intel(R) Core(TM) i9-14900K processor (3.20 GHz), 64 GB RAM, and a 64-bit operating system on x64 architecture.

### *2.5. Point cloud simplification method*

The method applied for point cloud simplification was increasing the minimum distance between points. This approach is implemented in software such as AutoCAD Civil 3D or CloudCompare. It is based on an iterative traversal of the points and checking the distance between a given point and the others. Although the intermediate results may vary depending on the order of point evaluation, the final outcome is always the same, since the initial and final points are fixed [21]. The organization of the point cloud does not change, as points are only removed rather than restructured. However, the surface generated from the simplified point cloud in the form of a TIN differs from the original, since it is

constructed without the deleted points. As a result, the generated surface produces different outcomes in the viewshed diagram.

Formally, let the original point cloud be defined as:

$$P = \{p_1, p_2, ..., p_n\}, \qquad p_i \in \mathbb{R}^3.$$

The goal of simplification is to select a subset $P' \subseteq P$ such that the minimum Euclidean distance between any two points in $P'$ is not smaller than a predefined threshold $\delta$:

$$P' = \{p_i \in P : \min_{q \in P', q \neq p_i} \|p_i - q\| \geq \delta\}.$$

Here, $\delta$ is the simplification threshold that determines the minimum allowed spacing between points.

For point clouds with densities of 4 to 20 points per square meter, the average spacing between points is typically on the order of several tens of centimeters. This spacing depends on the scanning geometry during data acquisition and it is not constant. Within a single square meter, distances between neighboring points can range from as little as 1 cm to as much as 70 cm [22]. The spacing is further influenced by the specific LiDAR sensor model employed. For the dataset used in this study, analysis showed that the minimum spacing between points was 4 cm, corresponding to an average density of 12 points per square meter.

During the simplification process, points closer to each other than a specified threshold $\delta$ were removed. Seven thresholds were defined:

$$\delta \in \{10\,\text{cm},\ 20\,\text{cm},\ 30\,\text{cm},\ 50\,\text{cm},\ 80\,\text{cm},\ 100\,\text{cm},\ 200\,\text{cm}\}.$$

For each of the simplified point clouds, a viewshed diagram was generated and compared against the reference diagram derived from the full, non-simplified dataset. The differences between them were analyzed. In addition, the computation times were recorded, including both the simplification stage and the viewshed diagram generation stage.

Increasing the minimum distance between points plays a central role in the simplification of point clouds. The specified distance thresholds allow control over the degree of simplification and its adaptation to the needs of the analysis. Higher thresholds result in sparser point clouds, which reduce detail but at the same time accelerate the generation of viewshed diagrams. Comparing viewshed diagrams obtained from different levels of simplification enables an evaluation of the effect of simplification on the accuracy of visibility analysis. Furthermore, incorporating the time required for point cloud simplification makes it possible to optimize the overall workflow of viewshed diagram generation with respect to both computational efficiency and analytical accuracy.

To evaluate the accuracy of the viewshed diagrams, three indicators were applied. The first one is the error rate, which measures the difference between the simplified and the reference (non-simplified) diagram. It is calculated by comparing individual pixels of both diagrams and expressed as the percentage of differing pixels relative to the total number of pixels in the image.

The second indicator concerns the magnitude of a single error. It quantifies the size of the area affected by an error, forming a contiguous patch. The larger the value of a single error, the greater its significance for the overall result, as it indicates a stronger influence on the analysis.

The third indicator covers an author-based visual–analytical assessment focusing on the visual interpretability of differences between the simplified and reference diagrams. The analysis was conducted by the authors and evaluated whether simplification-induced changes affected key visibility patterns, the spatial continuity of visible areas, and the presence or absence of critical occlusions relevant to viewshed interpretation. This analysis examined the extent to which these differences affect the correctness and interpretation of the results. In particular, it assessed whether changes introduced by simplification could distort or influence the understanding of spatial relationships visible in the reference diagram.

Together, these three indicators provide a more comprehensive evaluation of the quality of the simplified diagrams. The percentage error offers an objective measure of the differences, while the qualitative analysis addresses their potential impact on result interpretation.

## 3. Results

To evaluate the impact of point cloud simplification on visibility analysis, seven thresholds of minimum point spacing were tested: 10 cm, 20 cm, 30 cm, 50 cm, 80 cm, 100 cm, and 200 cm. The corresponding figures illustrate how the viewshed diagram changes depending on the adopted minimum distance between points. For each threshold, three key elements are presented:

- viewshed diagram: illustrates the simplified diagram at a given minimum point spacing,
- differences relative to the non-simplified diagram: highlights discrepancies between the simplified and the original, full-resolution diagram,
- significant differences marked in red: indicates differences with a substantial impact on the quality and accuracy of the diagram. These are highlighted in red for clarity.

Figure 3 shows the relationship between the error of viewshed diagrams and the adopted minimum distance between points. As the simplification threshold increases, the error systematically grows – from values close to zero for the full

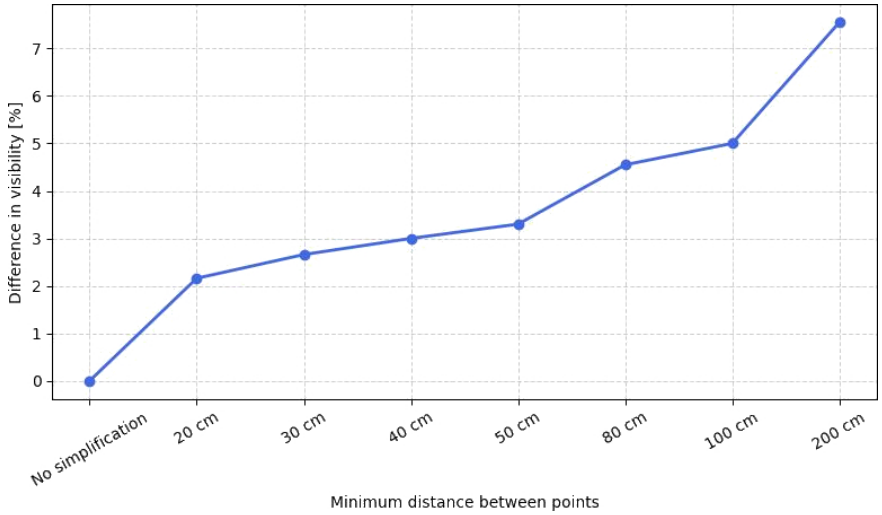


Fig. 3. Relationship between the percentage error in viewshed diagrams and the minimum distance threshold applied during point cloud simplification.

dataset up to more than 7.55 % for the 200 cm threshold. This demonstrates that excessive simplification leads to noticeable distortions in visibility analysis.

Figure 4 illustrates the number of points remaining in the cloud after applying different simplification thresholds. A sharp decrease can be observed – from nearly 80 million points without simplification to fewer than 1 million points at the 200 cm threshold. These results clearly confirm that the method effectively reduces the complexity of the point cloud.

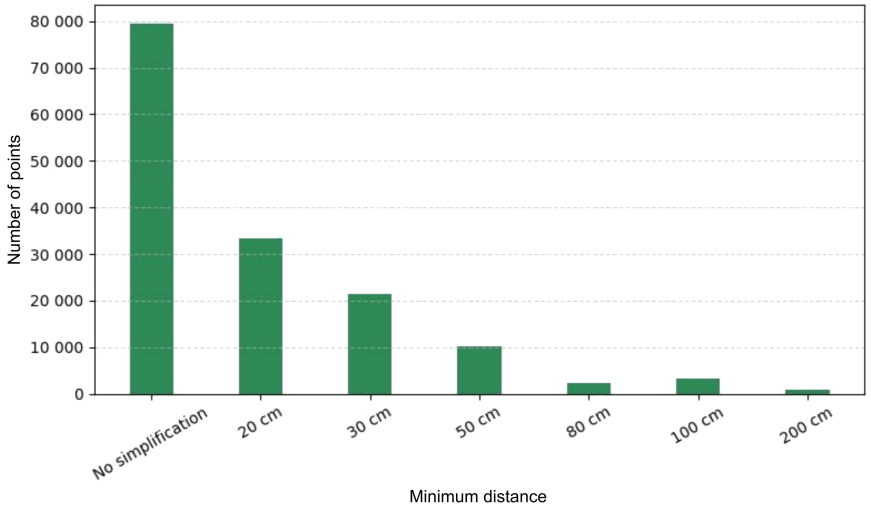


Fig. 4. Number of points in the point cloud as a function of the minimum distance between points.

Figure 5 presents the computation time required to generate viewshed diagrams depending on the degree of simplification. The results indicate that simplification significantly shortens computation time – from approximately 10 000 seconds for the full cloud to below 1000 seconds for the highest threshold. This means that reducing the number of points substantially improves computational efficiency, though at the cost of accuracy.

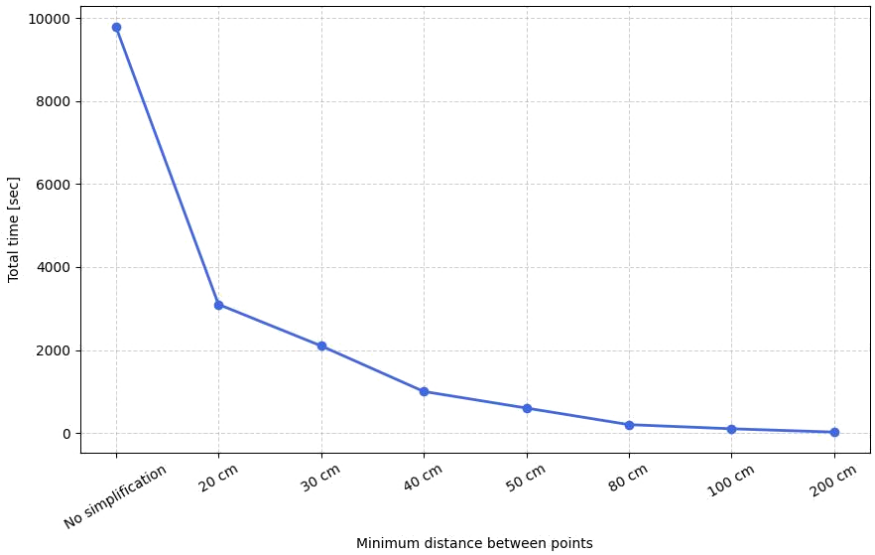


Fig. 5. Computation time required to generate a viewshed diagram as a function of the minimum distance between points in the point cloud, excluding the time needed for simplification and surface generation.

A summary of the numerical values is provided in Table 1, which lists the times of individual stages of viewshed diagram generation, the number of points

Table 1. Results of point cloud simplification for different minimum distances.

| Minimum distance [cm] | Simplification time [s] | Surface generation time [s] | Number of points | Simplification [%] |
|---|---|---|---|---|
| No simplification | 0 | 71 | 79 477 954 | 100.00 |
| 20 | 41 | 42 | 33 435 357 | 42.07 |
| 30 | 43 | 21 | 21 370 480 | 26.89 |
| 40 | 50 | 15 | 15 000 000 | 18.90 |
| 50 | 58 | 10 | 10 236 052 | 12.88 |
| 80 | 48 | 4 | 2 398 782 | 3.02 |
| 100 | 45 | 4 | 3 327 330 | 4.19 |
| 200 | 18 | 0 | 854 506 | 1.08 |

for different minimum distance thresholds, and their percentages relative to the original point cloud.

Table 2 presents a comparison of visibility differences resulting from the level of point cloud simplification. It can be observed that the greater the degree of simplification, the more significant the differences in the results become. This leads to a reduction in the consistency of the visibility map compared to the reference map, which was generated from the full, non-simplified point cloud.

Table 2. Difference in visibility results as a function of the minimum distance threshold.

| Minimum distance between points [cm] | Difference in visibility [%] |
|---|---|
| No simplification | 0.00 |
| 20 | 2.16 |
| 30 | 2.66 |
| 40 | 3.00 |
| 50 | 3.30 |
| 80 | 4.55 |
| 100 | 5.00 |
| 200 | 7.55 |

Reducing the minimum distance between points to 20 cm (Fig. 6) had only a minor effect on the accuracy of the viewshed diagram. The analysis showed that most areas remained unchanged, with the only noticeable differences occurring in regions of local forest density. This affected visibility only in a small portion of the area and had no significant impact on the overall quality of the diagram.

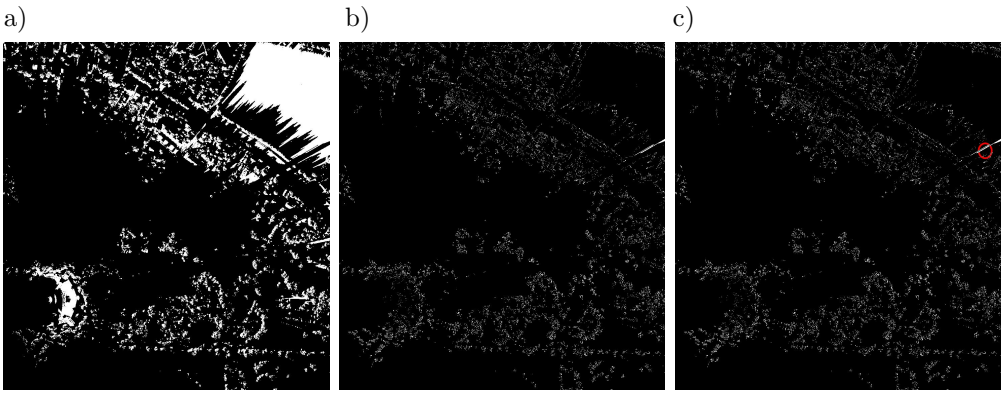


Fig. 6. Comparison of visibility analysis results for the 20 cm simplification threshold: a) viewshed diagram generated with a 20 cm minimum point spacing, b) differences compared to the reference (non-simplified) diagram shown as absolute visibility changes, c) significant differences highlighted in red.

A more detailed error analysis revealed that the difference amounted to only 2.16 % (Table 2) compared to the diagram generated from the full point cloud. Such a small discrepancy can be considered acceptable in the context of maintaining result precision.

In the following section, the analysis is based on absolute differences in visibility and is discussed using three complementary images. The first image presents the viewshed result generated with a given simplification threshold, the second shows absolute differences with respect to the reference (non-simplified) model, and the third provides the differences highlighted in red. These red markings are manual annotations made by the authors based on visual inspection and serve illustrative purposes. Their aim is to help the reader identify the most visually apparent discrepancies between the images. The markings do not result from automatic detection, and no magnitude threshold was applied.

The most substantial benefit of applying the 20 cm simplification threshold was the considerable improvement in computational efficiency. The computation time was reduced to 3042 seconds (Fig. 5), representing a significant acceleration compared to processing the full point cloud. This reduction enables faster generation of viewshed diagrams, which is particularly important in practical applications where data processing time is a critical factor.

Reducing the minimum distance between points to 30 cm (Fig. 7) resulted in a greater number of differences compared to the original chart. These differences were more noticeable; however, their impact on the overall quality and interpretation of the data remained minimal. Nevertheless, from the standpoint of accuracy and reliability of the data, it is recommended to carry out a detailed verification of these differences to ensure that they do not negatively affect the key conclusions drawn from the charts.

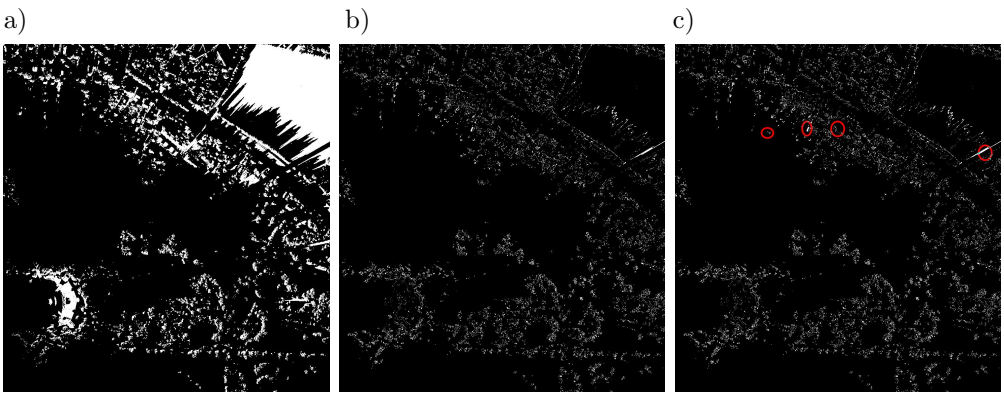


Fig. 7. Comparison of visibility analysis results for the 30 cm simplification threshold: a) viewshed diagram generated with a 30 cm minimum point spacing, b) differences compared to the reference (non-simplified) diagram shown as absolute visibility changes, c) significant differences highlighted in red.

An error of 2.66 % (Table 2) in relation to the original chart is higher than the previous 2.16 %, but it still falls within acceptable limits. This level of error is particularly permissible in the case of generating more extensive charts, where data processing speed may take precedence over absolute precision.

Reducing the distance between points to 30 cm also has a significant impact on computational performance. In practice, this means that the time required to generate the chart is just under 840 seconds (14 minutes) (Fig. 5), which is considerably shorter compared to the original 9660 seconds (161 minutes) (Fig. 5). As a result, despite the slightly higher error, this method can be effectively applied in scenarios where processing time is a key factor and minor deviations from ideal accuracy are acceptable.

In the case of a minimum distance of 40 cm (Fig. 8), the results begin to deviate dangerously from the original. In practice, this means that the accuracy of the generated data deteriorates significantly, resulting in an error exceeding 3 % (Table 2). Such a deviation may lead to incorrect conclusions and decisions based on these data.

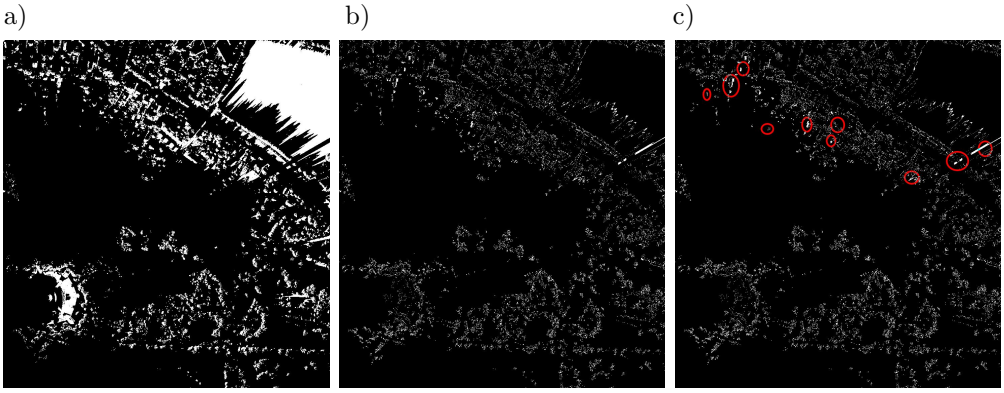


Fig. 8. Comparison of visibility analysis results for the 40 cm simplification threshold: a) viewshed diagram generated with a 40 cm minimum point spacing, b) differences compared to the reference (non-simplified) diagram shown as absolute visibility changes, c) significant differences highlighted in red.

Although the difference between 2.66 % and 3.0 % is small, exceeding the 3 % threshold causes noticeable changes in the nature of errors larger clusters of differences begin to appear (Figs. 7 and 8), leading to increased ambiguity in the interpretation of results. Based on this, it can be estimated that the acceptable error threshold is approximately 3 %, because above this value we observe a significant deterioration in the quality of the analysis.

Therefore, it is recommended that charts created using this distance be treated only as auxiliary charts supporting the main analysis, but not as the primary result. Auxiliary charts may be useful for quickly estimating trends or

general tendencies, but due to the higher level of error, they should not be used for making critical decisions. In cases where precision is crucial, methods with smaller point spacing should be relied upon, as they ensure greater accuracy.

Reducing the minimum distance between points to 50 cm (Fig. 9) caused a significant decrease in the number of points, reducing them to only 12 % of the initial amount. Such a loss of data has serious consequences for the quality of the chart. On the viewshed chart, an increasing number of differences appeared in comparison to the original chart, which resulted in an error of 3.3 % (Table 2).

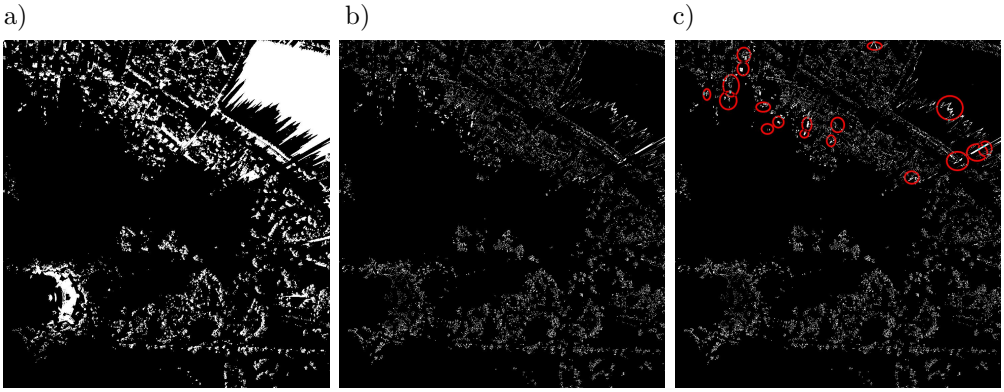


Fig. 9. Comparison of visibility analysis results for the 50 cm simplification threshold: a) viewshed diagram generated with a 50 cm minimum point spacing, b) differences compared to the reference (non-simplified) diagram shown as absolute visibility changes, c) significant differences highlighted in red.

An error level of 3.3 % indicates considerable deviations from the actual state of the analysis. Such a large discrepancy may distort the results and lead to incorrect conclusions; therefore, the chart obtained with this level of point reduction should be treated only as a supporting tool. It cannot be used as an accurate representation of the actual state of the analysis due to the substantial loss of information and potential interpretative errors.

Using a chart based on such a significantly reduced number of points may only be justified in situations where quick orientation in the data is required or where other methods are not feasible. However, for precise and reliable analyses, it is necessary to retain a larger number of points to ensure an accurate representation of the actual state of the analyzed objects or phenomena.

Reducing the minimum distance between points to 80 cm (Fig. 10) drastically shortens the time required to generate the viewshed chart. Compared to the full dataset, this time becomes almost negligible, which can be a major advantage in situations requiring rapid data processing. However, this substantial gain in performance comes with serious compromises in accuracy.

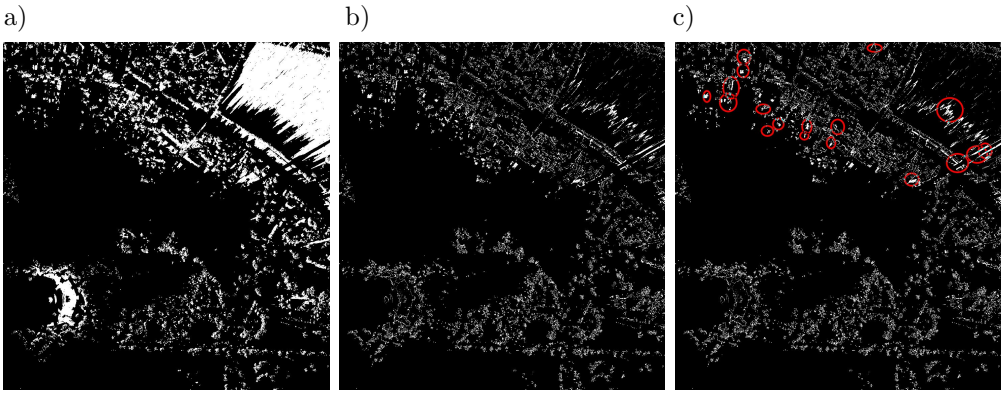


Fig. 10. Comparison of visibility analysis results for the 80 cm simplification threshold: a) viewshed diagram generated with a 80 cm minimum point spacing, b) differences compared to the reference (non-simplified) diagram shown as absolute visibility changes, c) significant differences highlighted in red.

An error exceeding 4.55 % (Table 2) means that the simplified chart diverges significantly from the chart based on the full dataset. In practice, this indicates that the differences between the simplified chart and the original are numerous and may lead to incorrect conclusions. Such a level of inaccuracy can introduce substantial distortions in data interpretation, which in turn may affect decisions made based on these charts.

Therefore, viewshed charts generated with a minimum point spacing of 80 cm should be regarded as quick, preliminary analytical tools. They can be useful for gaining a rapid overview of the data and guiding subsequent steps of analysis by highlighting areas that require closer examination. However, for precise and reliable analyses, it is necessary to create more detailed charts with smaller minimum point spacing to ensure full consistency with the original and to avoid significant errors.

Reducing the minimum distance between points to 100 cm (Fig. 11) significantly shortened the time required to generate the viewshed chart, reducing it to just 65 seconds (Fig. 5). Although this result is highly advantageous in terms of performance, it comes with serious compromises in data accuracy.

An error level of 5 % (Table 2) indicates a substantial deviation from the chart based on the full dataset. The numerous differences between the simplified chart and the original may lead to incorrect conclusions and distortions in data interpretation. Such a level of error is too high for the chart to be considered reliable for precise analysis.

In practice, this means that charts generated with a minimum point spacing of 100 cm may only be useful in situations requiring rapid data orientation or as supporting tools. They can serve for preliminary analysis and for identifying

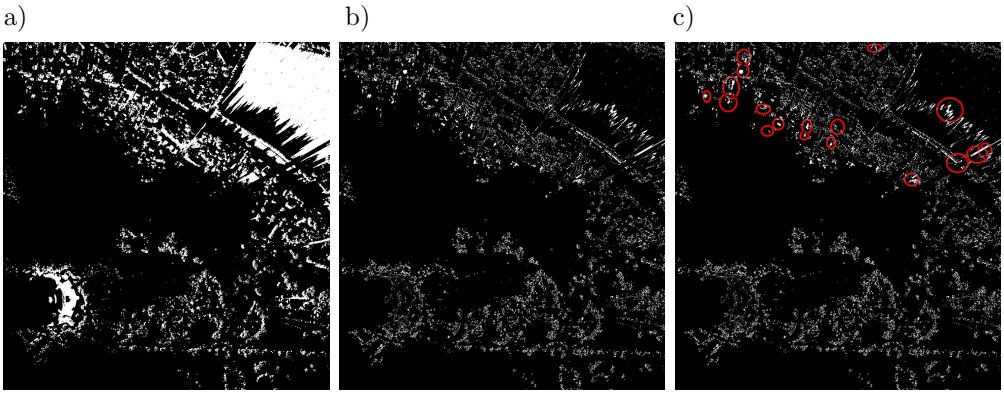


Fig. 11. Comparison of visibility analysis results for the 100 cm simplification threshold: a) viewshed diagram generated with a 100 cm minimum point spacing, b) differences compared to the reference (non-simplified) diagram shown as absolute visibility changes, c) significant differences highlighted in red.

areas that require closer examination, but they should not be used as the primary tool for drawing conclusions.

To ensure accuracy and reliability of analyses, it is necessary to use charts with smaller minimum point spacing. Only then can significant errors be avoided and results guaranteed to be sufficiently precise and representative of the actual state of the analyzed data.

Reducing the minimum distance between points to 200 cm (Fig. 12) leads to extremely fast generation of the viewshed diagram, taking only 12 seconds (Fig. 5). While such a short processing time may seem appealing, it comes with serious compromises in terms of data accuracy and reliability.

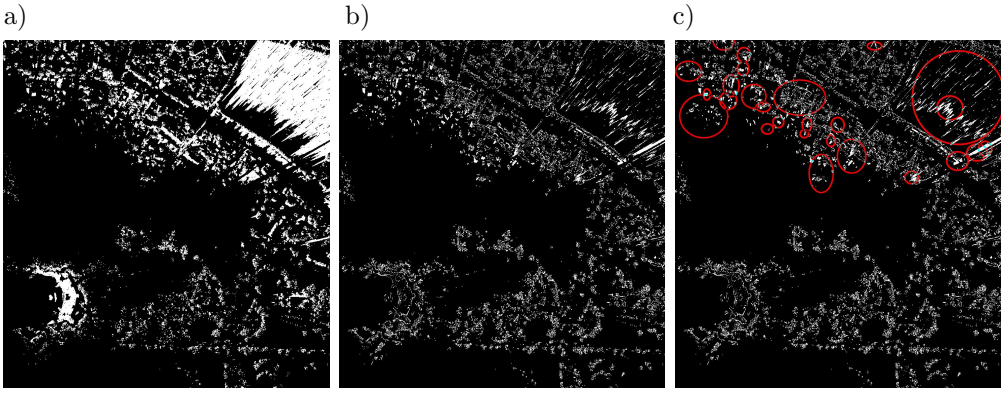


Fig. 12. Comparison of visibility analysis results for the 200 cm simplification threshold: a) viewshed diagram generated with a 200 cm minimum point spacing, b) differences compared to the reference (non-simplified) diagram shown as absolute visibility changes, c) significant differences highlighted in red.

An error level of 7.55 % (Table 2) relative to the reference chart is significant and indicates severe deviations from the actual state. The missing elements on the chart, marked in red, show which data areas were omitted or distorted. This drastically reduces the quality of the presented results, rendering the chart unreliable and unsuitable for analysis.

The absence of visible objects on this chart means that many essential pieces of information are missing, which disqualifies it as an analytical tool. In the context of any precise work, where accuracy and data completeness are critical, such a chart fails to meet the basic requirements.

## 4. Conclusions

The conducted research demonstrated that the degree of point cloud simplification, achieved by increasing the minimum distance between points, has a direct and measurable impact on both the accuracy of viewshed diagrams and the time required for their generation. The obtained results allow for identifying clear thresholds of analytical usability. For small simplification parameters ($\delta = 20$ cm to 30 cm), differences compared to the reference diagram do not exceed 2.16 % to 2.66 %, while the number of points is reduced to approximately 27 % to 42 % of the original dataset and computation time decreases from about 9600 s to a range of 840 s to 3000 s. This range represents an optimal compromise between accuracy and computational efficiency and can be recommended for reliable visibility analyses. Further increasing the simplification level ($\delta = 40$ cm to 50 cm) leads to errors exceeding 3 % and the emergence of noticeable spatial clusters of differences, which limits the interpretability of results. In such cases, diagrams may serve only as auxiliary or indicative tools. Simplifications of $\delta \geq 80$ cm result in significant distortions (errors of 4.55 % to 7.55 %) and should not be applied in analyses requiring high reliability. Future research should extend the analysis to other point cloud reduction methods, including adaptive approaches that locally decrease point density in areas of lesser importance for visibility while preserving detail in critical zones. Such solutions could enable further reduction of computation time without substantial loss of result quality.

## References

1. Orlof J., Point cloud based viewshed generation in AutoCad Civil 3D, *Technical Transactions*, **12**: 143–155, 2017, https://doi.org/10.4467/2353737XCT.17.215.7758.

2. Ozimek A., Ozimek P., Bohm A., Wańkowicz W., Planowanie przestrzeni o wysokich walorach krajobrazowych przy użyciu cyfrowych analiz terenu wraz z oceną ekonomiczną, Wydawnictwo PK, 2013.

3. Orlof J., Chmura punktów – nowa struktura danych, *Aura*, **12**: 3–6, 2017.

4. Orlof J., Ozimek P., Tin surface and radial viewshed determination algorithm parallelisation on multiple computing machines, *Symmetry*, **13**(3): 424, 2021, https://doi.org/10.3390/sym13030424.

5. Widłak A., Orlof J., Ray tracing and bound block elimination methods for viewshed analysis with efficiency enhancements through radial segmentation and parallel processing, [In:] *Proceedings of the 39th European Conference on Modelling and Simulation (ECMS 2025)*, European Council for Modelling and Simulation, pp. 631–637, 2025, https://doi.org/10.7148/2025-0631.

6. Rubinowicz P., Sustainable development of a cityscape using the visual protection surface method – optimization of parameters for urban planning, [In:] D. Holzer, W. Nakapan, A. Globa, I. Koh [Eds.], *RE: Anthropocene, Design in the Age of Humans – Proceedings of the 25th CAADRIA Conference – Volume 1*, Chulalongkorn University, Bangkok, Thailand, 5–6 August, pp. 863–872, 2020, https://doi.org/10.52842/conf.caadria.2020.1.863.

7. Lv C., Lin W., Zhao B., Approximate intrinsic voxel structure for point cloud simplification, *IEEE Transactions on Image Processing*, **30**: 7241–7255, 2021, https://doi.org/10.1109/TIP.2021.3104174.

8. Moenning C., Dodgson N.A., A new point cloud simplification algorithm, [In:] *Proceedings of the 3rd International Conference on Visualization, Imaging and Image Processing (VIIP 2003)*, Benalmádena, Spain, 8–10 September, pp. 1027–1033, 2003.

9. Ding Z., Li R., Point cloud reduction method based on curvature grading and voxel filtering, *Journal of Electrical Systems*, **20**(2): 318–326, 2024, https://doi.org/10.52783/jes.1180.

10. Wu T., Yang F., Farooq U., Hao H., Li Y., Diao G., A new point cloud simplification method for reducing visual distortion, *Measurement*, **229**: 114400, 2024, https://doi.org/10.1016/j.measurement.2024.114400.

11. Wang S. *et al.*, A new point cloud simplification method with feature and integrity preservation by partition strategy, *Measurement*, **197**: 111173, 2022, https://doi.org/10.1016/j.measurement.2022.111173.

12. Geoportal Krajowy, available online https://mapy.geoportal.gov.pl/imap/Imgp_2.html [accessed: 07.09.2025].

13. Zhou Q., Digital elevation model and digital surface model, [In:] *International Encyclopedia of Geography: People, the Earth, Environment and Technology*, D. Richardson, N. Castree, M.F. Goodchild, A. Kobayashi, W. Liu, R.A. Marston [Eds.], pp. 1–17, 2017, https://doi.org/10.1002/9781118786352.wbieg0768.

14. Kurczyński Z., Bakuła K., Generowanie referencyjnego numerycznego modelu terenu o zasięgu krajowym w oparciu o lotnicze skanowanie laserowe w projekcie ISOK, Archiwum Fotogrametrii, Kartografii i Teledetekcji, *Techniki Pomiarowe*, **23**: 59–68, 2013.

15. Negishi J.N. *et al.*, Using airborne scanning laser altimetry (LiDAR) to estimate surface connectivity of floodplain water bodies, *River Research and Applications*, **28**(2): 258–267, 2010, https://doi.org/10.1002/rra.1442.

16. Gao X., Chang Z., Ma C., Qu M., Zhang S., Xiao F., Accuracy comparison and analysis of interpolation methods in DEM generation with 3D laser point cloud data, [In:] Proceedings of the International Conference on Remote Sensing, Mapping, and Geographic Systems (RSMG 2023), Kaifeng, China, Vol. 12815, 128150C, 2023, https://doi.org/10.1117/12.3010326.

17. Zhang H. *et al.*, Deep learning-based 3D point cloud classification: A systematic survey and outlook, *Displays*, **79**: 102456, 2023, https://doi.org/10.1016/j.displa.2023.102456.

18. ASPRS, *LAS Specification*, The American Society for Photogrammetry & Remote Sensing, Baton Rouge, LA, 2019.

19. Tandy C.R.V., The isovist method of landscape survey, [In:] *Methods of Landscape Analysis*, H.C. Murray [Ed.], Landscape Research Group, pp. 9–10, London, 1967.

20. Benedikt M.L., To take hold of space: Isovists and isovist field, *Environment and Planning B*, **6**(1): 47–65, 1979, https://doi.org/10.1068/b060047.

21. Moenning C., Dodgson N., Intrinsic point cloud simplification, [In:] *Proceedings of the 14th GrahiCon*, Moscow, Russia, 6–10 September, Vol. 14, 8 pages, 2004.

22. Petras V., Petrasova A., McCarter J.B., Mitasova H., Meentemeyer R.K., Point density variations in airborne lidar point clouds, *Sensors*, **23**(3): 1593, 2023, https://doi.org/10.3390/s23031593.

*Received September 18, 2025; revised December 22, 2025; accepted December 22, 2025; available online December 23, 2025; version of record February 9, 2026; published issue March 17, 2026.*

*Computer Assisted Methods in Engineering and Science*
**33**(1): 69–81, 2026, https://doi.org/10.24423/cames.2025.273

# Possibilities for Obtaining Terrain Models, Orthophoto Maps, and Point Clouds with the Use of a Multirotor UAV

Piotr Łabędź, Paweł Ozimek*

*Cracow University of Technology, Kraków, Poland*
** Corresponding Author: pawel.ozimek@pk.edu.pl*

In this paper, a method for acquiring spatial data using unmanned aerial vehicles (UAVs) is presented. In this work, the UAV is a hexacopter equipped with a high-end camera capable of recording 4K video and capturing high-resolution photographs.

The first step in data acquisition involves conducting a flight over the analyzed object, which can be either a land area or a construction site. During the flight, a series of photographs or video footage is recorded. In a later stage, these recordings are processed with the use of appropriate software. This processing consists of several steps. First, the recorded photos are arranged according to their location of capture and then properly stitched together. Based on this, a dense point cloud is created, from which it is possible to build a mesh with an adjustable number of vertices. In addition, the polygons' textures are extracted from the photographs taken.

According to this approach, it is possible to obtain high-quality data for both terrain and architectural objects. The resulting point cloud can serve as a starting point for performing a variety of analyses or inventories, provide the basis for high-precision models or supplement existing lower-density point clouds.

**Keywords:** landscape architecture, terrain modeling, orthophoto map, point cloud, multirotor.



## 1. Introduction

In the era of geographic information systems (GIS), building information models (BIMs), and computer integration of manufacturing (CIM), which are used to carry out various spatial analyses, spatial planning, architectural and urban design, or landscape architecture, adequate quality and quantity data are required. Modern computers and workstations are capable of processing large datasets, although specialized software rarely takes full advantage of these capabilities.

There are many research programs aimed at acquiring spatial data, which has made it possible to create terrain models, represent land coverage, individual objects, vegetation, or even individual trees. These data are obtained using satellites, planes, drones, or terrestrial scanners. Thanks to the existence of programs such as Copernicus [1] and Sentinel [2], which collect data by using satellites, vast amounts of information have been accumulated that can be used, e.g., to measure building subsidence in areas affected by mining activity. These datasets are very accurate and can be updated continuously. However, the mentioned programs are carried out with considerable resources, and so far their effects have not been used to the extent that would justify the investment. The environment of landscape architects, professionals involved in spatial planning, and urban planners should make full use of these data.

In the databases of geodesy and cartography centers, there are spatial data available at different densities. These data concern both terrain models and land coverage. For many data formats, such as systematic point grids, point clouds are obtained using various remote sensing methods. Landscape files that are interesting for landscape architects are LAS files containing point clouds acquired using LIDAR [3]. Simply put, these files contain sets of points specified by $x$, $y$, and $z$ coordinates, along with color information in the additive red, green, and blue (RGB) model [4]. In addition, the points in these files are classified into four layers: ground, building, water, and high vegetation. As part of the Informatyczny System Osłony Kraju (ISOK – National Protection Information System) project [5], a surface scan of Poland was carried out, resulting in a point cloud in two density standards covering 93 % of the country's area. These data, however, age and become outdated. Relatively often, there is a need to supplement them. In such cases, spatial scanning technology can be useful, especially when using a multirotor UAV equipped with a high-precision camera.

## 2. Technology

Filling in gaps or updating spatial data should be performed with the use of native formats that are appropriate for the given environment. Point clouds should be supplemented with sets of points included in this structure. Therefore, it is necessary to obtain such a set by scanning limited areas or specific objects. Each point should have coordinates in the correct layout and standard color information. This type of structure can be obtained using photogrammetric technology. In this technology, while eye-level photographs can be used, more complete information is obtained through the use of drones. To capture precise images from specific points in space, multirotors are used, as they can hover anywhere in the air and fly at very low speeds.

In this research, a hexacopter equipped with a Lumix GH-4 mirrorless camera is used. This camera is mounted on a 3-axis brushless gimbal (a stabilizer that enables the camera to rotate independently of the carrier's movements; in this case, the carrier is the multirotor), which ensures perfect stabilization of the recorded image. The camera can record photos up to $4608 \times 3456$ pixels and videos in $4096 \times 2160$ pixels (4K standard) at 25 fps. The hexacopter and gimbal are controlled separately using radio equipment. Although this separation of the aircraft operator and camera operator functions allows for greater precision in flight and camera control, it involves the need for two operators to control it. According to Polish law, flights performed with UAVs for purposes other than recreational require operators to have a qualification certificate issued by the Civil Aviation Office. It is also necessary to review the airspace layout in the area of planned flights. In some zones, it is necessary to obtain consent from the administrator of the given space, e.g., in areas near airports, strategic industrial facilities, or national parks.

Data acquisition consists of performing a flight over the object while simultaneously taking photographs. Attention should be paid to the aspects of proper recording parameters – sensor sensitivity, white balance, focus point, aperture value, and exposure time for each frame. The type of flight depends on the type of object being surveyed. An architectural object should be registered from a low altitude with the camera set horizontally or at a slight angle of inclination relative to the object. On the other hand, terrain should be recorded from a higher altitude with the camera pointing vertically downward. The specific flight altitude also depends on the type of airspace in which the flight is performed.

During the flight, a series of photographs is taken, which should be made in such a way that neighboring shots contain a common fragment of the photographed object. This requires the multirotor to pause in places suitable for taking each picture. Another approach is to record the footage continuously throughout the whole flight. The recorded sequence should be divided into individual frames, as they are the starting point for further processing. Neighboring frames, as in the case of a series of photographs, should contain a common fragment of the analyzed object and also be correctly registered. This applies in particular to avoid the blur effect, which often occurs during flights at excessive speed. Thanks to the high-quality gimbal used on the multirotor, it is possible to minimize distortions of photographs caused by the unstable flight of the aircraft. The stabilization of the gimbal, combined with the stabilization of the lens in the camera, almost completely reduces vibrations associated with flight, even under adverse weather conditions such as gusts of wind.

In this study, the second method is employed – the recording of video material. The recorded video is then automatically divided into individual frames, from which some of them are selected for further processing. Frame selection

for further processing can be carried out by the operator, assisted by an initial automatic selection of frames at regular intervals (e.g., every 25 frames, corresponding to 1 second of video). The criteria for selecting frames are discussed in the final part of this article.

## 3. Model generation procedure

The Agisoft Metashape software was used to create the point cloud and 3D model. The first step in the creation procedure is to import the previously prepared frames. These frames are then analyzed to ensure that sufficient EXIF (exchangeable image file format – a metadata standard used for storing information about image and sound files, including camera settings, date, time, and location) data, such as the focal length of the camera, are available. When this data is not available, the program assumes that the photo was taken using an equivalent focal length of 50 mm. The imported photos must then be aligned. During this phase, common points appearing in the analyzed pictures are identified, and the position and spatial orientation of the camera are determined based on these matches. The result is a set of reconstructed positions of each photograph taken and a sparse point cloud, usually containing tens or hundreds of thousands of points (Fig. 1). Although this is a relatively small number of points and limits its usability, the sparse cloud can be exported to external programs and further processed at this stage.

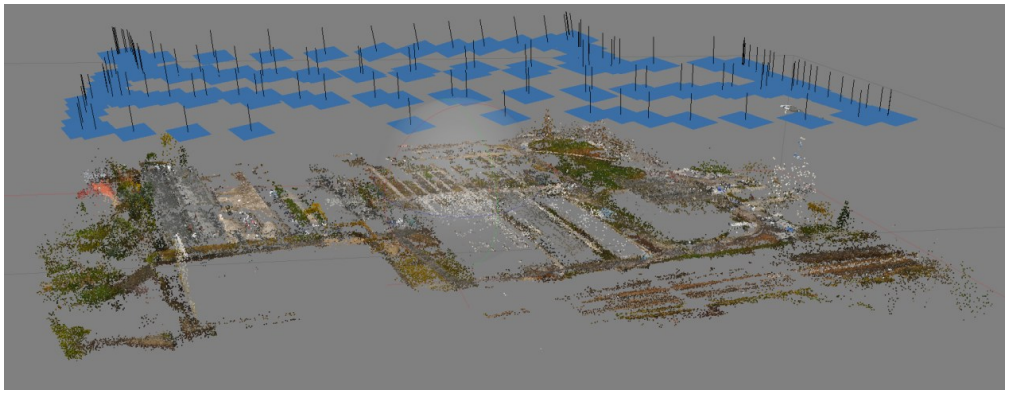

Fig. 1. Example of a sparse point cloud (containing 130 000 points) with visible designated camera positions.

The next stage of the procedure is the construction of a dense point cloud (Fig. 2). In this phase, the software calculates depth information based on the information obtained from the estimated shooting position. It is possible to generate a very dense cloud containing tens of millions of points. Such a cloud

Fig. 2. Example of a dense point cloud containing over 53 million points.

may already form a basis for further editing or analysis. It is also possible to classify the points in the generated cloud, e.g., based on color information.

Both dense and sparse point clouds can become starting points for creating a 3D mesh. The number of polygons in this mesh can be defined automatically as a fraction of the number of points in the cloud or can be arbitrarily determined by the user. Thanks to properly calibrated photographs, it is possible to capture the geometric structure of the model but also the color information of individual polygons, which can be saved in the form of texture.

## 4. Case studies

During the research, attempts were made to obtain data for three different facilities – an open area, a built-up area, and a detached building. Each of these cases required an individually tailored approach to data acquisition.

### *4.1. Case 1 – open area*

As an example of an unbuilt area, a fragment of the open area near Skotnicka Street in Kraków was chosen. This area is a small hill covered with grass on the ridge and bushes and trees on the slopes. For this case, the acquisition of data involved flights at an altitude of 100 m above ground level (AGL) – the maximum available height in the given area. The camera of the UAV was directed vertically downward, and three flights were conducted along parallel strips of space, several meters apart (Fig. 3).

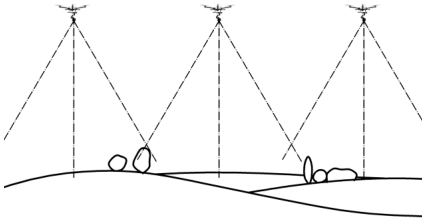

Fig. 3. Data acquisition in open areas.

This method of acquisition allowed the registration of both the terrain details and its coverage (Fig. 4). The accuracy of vegetation registration, however, depends on the way it is spatially arranged. Shrubs growing close to each other, forming coppices, were recorded correctly, while vegetation elements growing as individual objects often contained blank spaces. This limitation is associated with the acquisition method used.

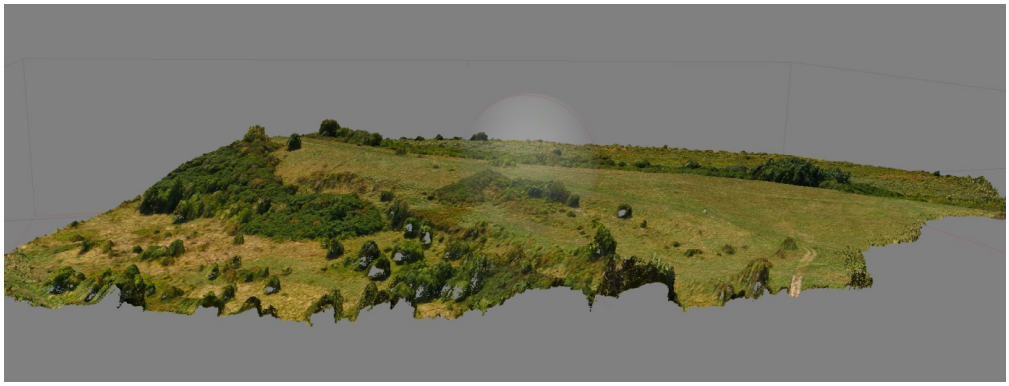

Fig. 4. Fragment of a dense point cloud of the open area (about 5 million points). The illustration clearly shows blank spaces.

If it is necessary to fill these blank spaces, it is essential to accurately photograph the given object, especially from the side where the gaps occur (Fig. 5).

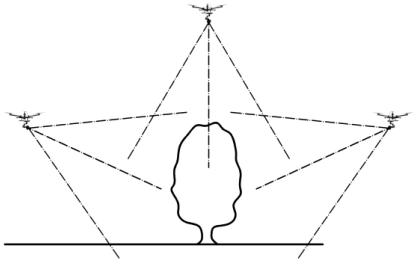

Fig. 5. Filling in the gaps of a single object.

Based on stitched photos, it is also possible to obtain a highly detailed orthophoto map. If the map is georeferenced, it can be used as a GIS layer (Fig. 6).

Fig. 6. Fragment of an orthophoto map generated from stitched photos.

### *4.2. Case 2 – built-up area*

As a case study, the built-up area of the University of Agriculture in Kraków was selected. The campus is located a short distance north of Kraków's city center and comprises research and teaching facilities, student dormitories, a sports hall, and specialized infrastructure such as a greenhouse and crop plots. The architectural ensemble dates to the second half of the 20th century and reflects a modernist style, characterized by simple geometric forms and minimal decorative elements. Data acquisition using a multirotor in built-up areas requires detailed knowledge of the specific characteristics of the area being analyzed. First of all, as already mentioned, legal restrictions regarding flights in the given airspace must be taken into account. It is also necessary to analyze the distribution of all types of terrain and construction obstacles, such as trees, tall buildings, overhead transmission lines, chimneys, or construction cranes. Data acquisition in the analyzed case involved flights at an altitude of about 50 m AGL, which was determined by weather conditions prevailing at the time. The camera was directed vertically downward, similar to the data acquisition procedure in the open area. Video recording took place along parallel strips of space.

The obtained point cloud was characterized by great detail of all elements of the terrain, clearly visible directly from above, such as roofs, the ground or parked cars. However, the surfaces of building walls were reproduced very poorly or not captured at all (Fig. 7). Again, this limitation is related to the chosen acquisition method. Supplementing data for building walls would require a different approach, described in the next section. Certain inaccuracies were also observed for objects largely covered with transparent material, such as greenhouses.

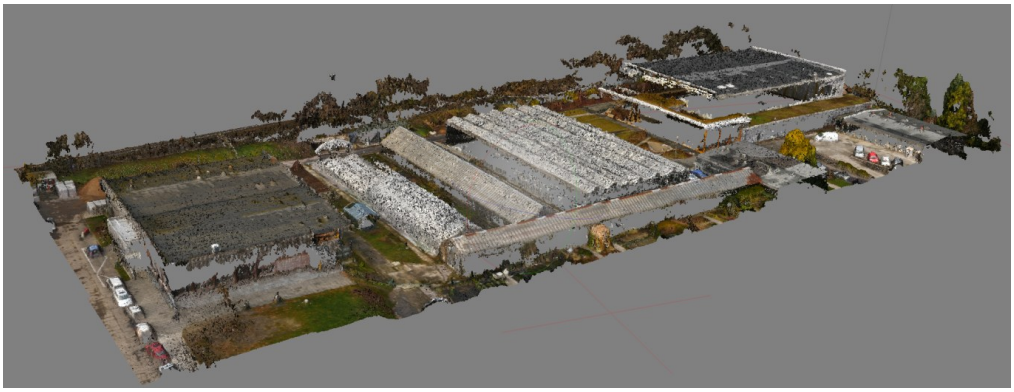

Fig. 7. Fragment of a dense point cloud of the built-up area (about 23 million points).

### *4.3. Case 3 – detached building*

The Houston teaching and administration building, located on Warszawska Street and forming part of Cracow University of Technology (CUT), was selected as the representative detached structure. It accommodates the dean's offices, laboratories, and lecture halls, making it a significant component of the CUT campus. Obtaining data on the whole structure of a single architectural object requires a slightly different approach than those presented in the previous two cases. Although a flight directly above the object with the camera pointing downward is necessary to record the details of the roof of the object, it is more important to collect information about the building's walls. In addition to the hazards described in the previous cases, another important element to be taken into account during the flight is the proximity of surrounding buildings. Their location can significantly hinder or even prevent proper data acquisition. The construction of the multirotor and its control system necessitates the use of a camera with a fixed focal length. The only way to change the cropping, in this case, is to change the position of the camera, and thus reposition the multirotor itself. Consequently, the registration method required flying around the analyzed object with the camera directed towards its walls. Correct registration of the roof edge requires framing that simultaneously captures both the

roof and the part of the wall beneath it. This forces a diagonal orientation of the camera relative to the object (Fig. 8).

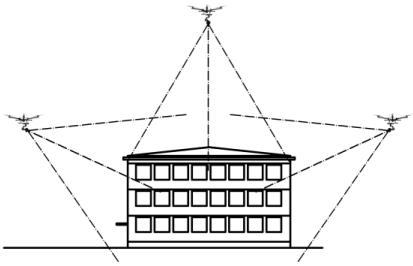

Fig. 8. Data acquisition of an architectural object.

In the case of an architectural object, one of the main requirements is to obtain the highest possible level of detail in reproduction. The problem, in this case, is the presence of relatively small elements (in relation to the whole building size) protruding from the main structure, such as antennas, chimneys, or air-conditioning installations. While the overall shape of the building was reproduced satisfactorily, the above-mentioned details were not captured consistently in all cases (Fig. 9).

Fig. 9. Fragment of a dense point cloud of an architectural object (about 7 million points).

From each point cloud, a polygon mesh can be obtained as well. This mesh may be based on either a sparse or a dense cloud, and the number of polygons it consists of can be determined arbitrarily (Fig. 10).

Transforming a point cloud into a polygon mesh reveals further issues that are not always clearly visible. While during point cloud inspection, most surfaces appear to be uniform, the polygon mesh model exposes significant surface irreg-

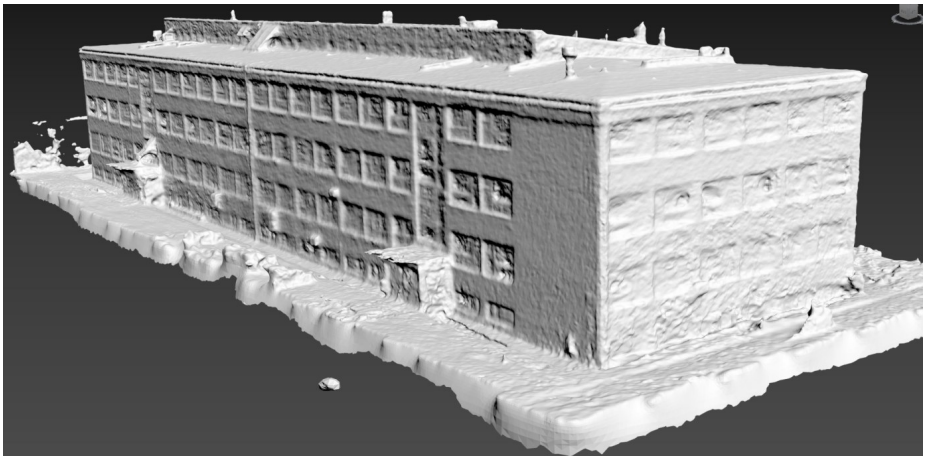

Fig. 10. Polygon mesh generated based on a dense cloud with an arbitrarily defined number of polygons.

ularities, located mainly in areas where transparent surfaces such as windows are present (Fig. 11).

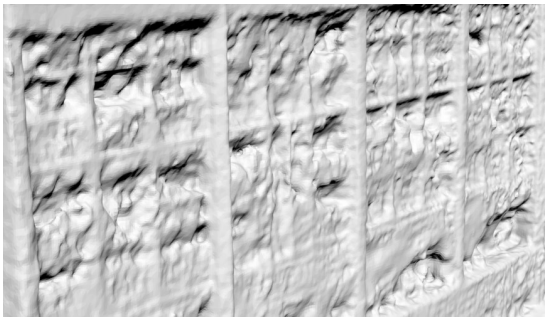

Fig. 11. Problems observed when processing objects that contain transparent and reflective surfaces.

## 5. Supplementing point clouds

The presented methods were used to supplement a point cloud containing scanned data obtained as part of the ISOK project. As an example, a fragment of the building of the Royal Palace in Łobzów was selected. After the procedures described in the previous paragraphs were carried out, a dense point cloud of one of the facades was obtained, containing over 2 million points (Fig. 12).

The resulting cloud was then scaled using a reference section and aligned through rotations with the existing point cloud containing data on the surrounding areas. After completing this alignment, both clouds were merged and can function as a single data structure (Fig. 13).

Fig. 12. Dense point cloud of the facade of the Royal Palace in Łobzów.

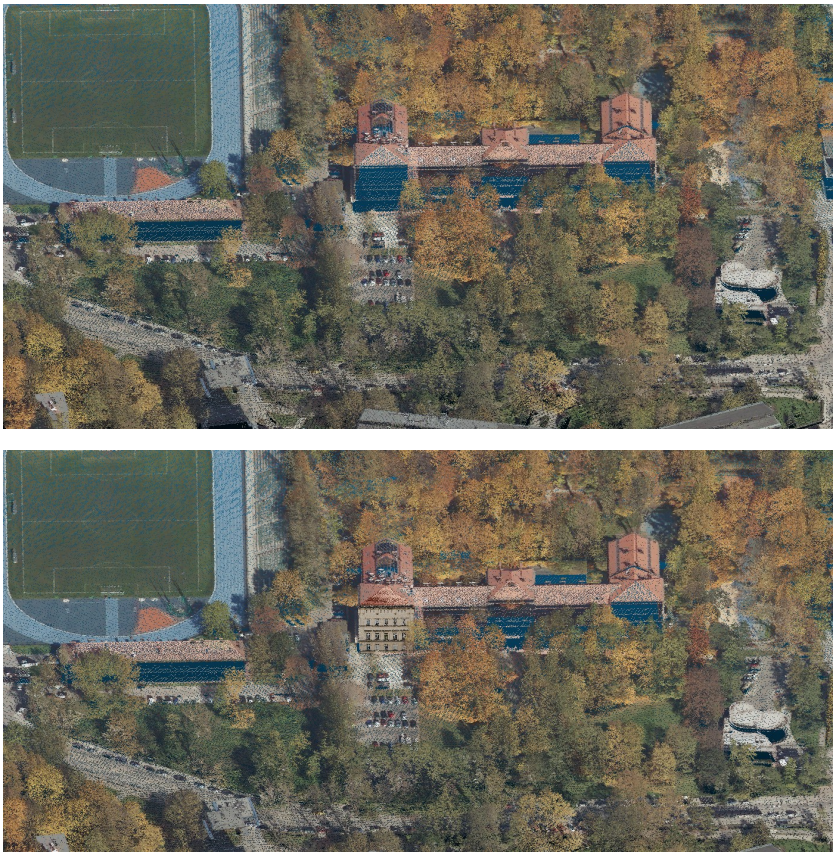

Fig. 13. Original (top) and supplemented (bottom) point cloud of the neighborhood of the Royal Palace in Łobzów.

The supplemented point cloud is denser than the original dataset, which is most evident in close-up views (Fig. 14).

Fig. 14. Close-up view of the point cloud of the neighborhood of the Royal Palace in Łobzów.

## 6. Discussion

This article presented a method for acquiring spatial data using UAVs. The presented procedure shows the process of building a point cloud without using ground control points or a predefined flight path. Using the presented methods, it is possible to supplement point clouds acquired using remote sensing methods with detailed data for smaller areas. The workflow enables the creation of both sparse and dense point clouds, polygon meshes with appropriate textures, as well as orthophoto maps.

The methods presented in the paper are not devoid of imperfections. During the processing of data obtained during the flight over the open area, there was a certain amount of blank spaces associated with the chosen acquisition method. These gaps required additional supplementation using another method, which in turn necessitated an additional field visit, as such errors only become apparent during data processing. In the case of architectural objects, errors related to the structure itself were visible, including reduced accuracy in the registration of small, angular elements, and problems in generating polygon meshes for transparent and reflective surfaces.

The procedure for recording video and photographic material also matters. Proper exposure of individual frames has a very large impact on the final quality of the generated point cloud. At present, research is underway to assess the impact of initial processing of input images on the final quality of the generated

models. In the presented work, video frames were chosen arbitrarily at intervals of 25 frames (corresponding to 1 second of flight). It seems necessary to develop a method for the automatic selection of appropriate frames in order to generate point clouds of optimal quality. One potential indicator that could be used for this purpose is the Tanimoto coefficient. Its application, along with comparisons to other methods of non-systematic frame selection are described in [6]. Such a procedure would also have to assess the suitability of specific photographs in terms of both exposure and focus, based on objective measures.

In this study, the merging of two point clouds was performed manually. In order to make the most of possibilities of supplementing existing datasets, a procedure should be devised to allow an automated alignment and merging. This would require having spatial coordinates for the newly created cloud, which is not trivial when the cloud is created from video material.

Spatial data in the form of point clouds is updated as part of the ISOK program and also through initiatives undertaken by local spatial management authorities. However, these updates do not keep pace with rapid changes of urban space, particularly in big cities. In addition, the purpose of such projects is usually to obtain data about the area for flood protection purposes. In the case of projects with a limited spatial extent, e.g., a single building or an urban square, higher-density data may be very useful. The method described in this article allows to supplement and harmonize the data available in geodetic institutions, and supports their use in precise context-specific design.

## References

1. Copernicus, https://www.copernicus.eu/en [access: 26.10.2025].
2. Sentinel Online, https://sentinel.esa.int/web/sentinel/home [access: 05.11.2025].
3. Ptak A., LiDAR w wielkim mieście, *Geodeta: Magazyn Geoinformacyjny*, **12**: 28–29, 2014.
4. Ozimek A., *Miara krajobrazu. Obiektywizacja oceny widoków i panoram wspomagana narzędziami komputerowymi*, Wydawnictwo PK, Kraków, 2019.
5. Informatyczny System Osłony Kraju, http://www.isok.gov.pl/ [access: 28.10.2025].
6. Skabek K., Łabędź P., Ozimek P., Bober K., Ozimek A., Zając P., Selecting images from UAV sequences for photogrammetric reconstruction, [In:] *ECMS 2025 Proceedings*, M. Scarpa, S. Cavalieri, S. Serrano, F. De Vita [Eds.], pp. 1–8, European Council for Modelling and Simulation, 2025, https://doi.org/10.7148/2025-0653.

*Received November 14, 2019; revised December 23, 2025; accepted December 23, 2025; available online December 23, 2025; version of record February 2, 2026; published issue March 17, 2026.*

# Contents